MI
Masonry International
Journal of the International Masonry Society
www.masonry.org.uk
2023

FEATURED IN THIS ISSUE:

- **Prediction of the Seismic Behaviour of an Iconic Masonry Pagoda in China**
- **On The Effective Stiffness of Slender Concrete Masonry Walls in the Canadian Masonry Standard**
- **Characterizing Bidirectional Interaction in Unreinforced Masonry Buildings by Pseudo Dynamic Hybrid Simulation**

ISSN 2398-757X Sfb (2) Fd,e,f UDC 62 + 69 Vol 35, No 2. 20-49 2023

The International Masonry Society

Registered Office: Lucideon Ltd, Queens Road, Penkhull, Stoke-on-Trent, ST4 7LQ, UK

Society website www.masonry.org.uk

Secretary: Mr P Wood
26 Widecombe Road, Birches Head, Stoke-on-Trent, ST1 6SL, UK
Tel: +44(0) 1782 279051
email: philip.e.wood@btinternet.com

IMS is an International Society with Members throughout the world. It provides a focus for all those involved in or interested in the manufacture of masonry materials, the design of masonry structures and their economical construction. All masonry units are included: calcium silicate, clay, concrete and stone together with mortar and the ancillary components, dpc's and straps, ties and fixings.

The Society's journal, *Masonry International,* is published three times each year. Each issue consists of original papers with the latest research findings, both experimental and analytical, practical papers, together with Society and International news. Each Member receives *Masonry International* free of charge. Corporate Members receive two copies. Members may purchase other publications, including the Proceedings, and attend meetings and conferences at preferential Members' rates. *Masonry International* is available to libraries and others on subscription.

Technical meetings are held from time to time at which original papers are presented, discussed and which subsequently may be published after peer review. Some of these meetings are major conferences, including the quadrennial International Masonry Conference.

Everyone with any interest in masonry should keep themselves up to date as a Member with the opportunity for discussion with one's peers. Membership is of special value to: architects, engineers, surveyors, builders, developers, manufacturers, teachers and research workers, users of masonry products and all those interested in the appearance and performance of the built environment.

Enquiries

Enquiries concerning membership, subscriptions to the journal and information concerning meetings should be addressed to the Secretary: Mr PE Wood at the postal or email address at the head of this page.

Payment

Cheques in sterling or bankers' drafts on a UK bank should be made payable to **THE INTERNATIONAL MASONRY SOCIETY.**

The Society also has the facility to accept the following credit cards: EUROCARD/MASTERCARD/VISA/AMERICAN EXPRESS.

Persons wishing to pay in this way should send their card number, date of expiry, the name as it appears on the card and the address together with a note authorising the sum to be debited and signed with the recognised signature. Payment can be made online at www.masonry.org.uk

NOTES FOR AUTHORS

Papers for publication in Masonry International should be sent by email to philip.e.wood@btinternet.com

Subject matter

Papers on any aspect of design, construction, maintenance, or research relating to masonry and masonry materials are invited for publication in Masonry International.

Format

Contributions should be formatted in accordance with the specified **template** prepared by the Society. This can be found on the **Society website, www.masonry.org.uk** as listed under Masonry International- Notes for Authors MI Paper – Template v4.DOC.

Copyright

If authors include in papers material which is not their copyright, for example figures and tables, they MUST not only give appropriate acknowledgement by way of references but also obtain the approval of the copyright holder for the Society to reproduce it.

Any queries relating to submissions should be addressed to the Secretary, contact details as above.

CITATION

Masonry International is an archival publication for original papers on research and practice in masonry materials, design and construction. All submissions to the Journal are refereed and edited. The Bulletin contains more practical papers and review articles. Material appearing in this publication, and in the separate Proceedings of the Society, has been subjected to peer review and, as such, may be cited and accepted as significant in relation to professional advancement.

Contents

Society News

International Review

Masonry Calendar

2024

- 18th International Brick and Block Masonry Conference, University of Birmingham. 21-24 July 2024.
- TMC -2024 Annual meeting – Virtual – 16-19 October 2024

2026

- 11th International Masonry Conference (11th IMC) July 2026

Publications

Refereed Papers

Cover Picture

Masonry outstand on corner of Grimmalsche and Nikolai Strasse in Leipzig, Germany.

POSTAL ADDRESSES OF THE SOCIETY
The main postal address of the Society is that of the Secretary.
Secretary: Mr PE Wood, 26 Widecombe Road, Birches Head, Stoke-on-Trent, ST1 6SL, UK
OR by email to philip.e.wood@btinternet.com
Accounts and Administration: Mrs J C Wood, 26 Widecombe Road, Birches Head, Stoke-on-Trent, ST1 6SL.
Tel: +44 (0) 1782 279051; Email: julie.c.wood@btinternet.com
Executive Editor: Dr A N Fried

Society News

Obituary: Denzil Sencer

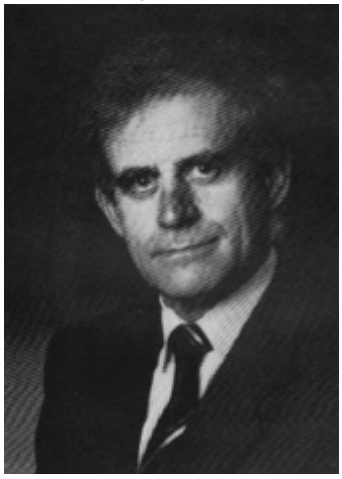

It is with deep sadness that the Society learnt of the passing of Denzil Spencer earlier this year. Many of the Society members will recall that Denzil was President of the Society in 1992-93. He was born at Blyth in North Nottinghamshire in 1943. After graduating in applied chemistry from Loughborough University of Technology, where he was awarded a 1st Class Honours Degree, he joined the Steetley organsation Research Department in Worksop. He was later awarded a Ph.D at Loughborough University after studying the high temperature properties of Magnesia. He continued his career at Steetley to become Technical Director in 1973 of Ceramics Division. In 1980, he was appointed Managing Director of the Ceramics Division and then Operations Director for Steetley Refractories. Eventually, he transferred to Steetley Brick developing his career to coincide with the start of the Company's major investment programme, to become Managing Director of Steetley Brick and Concrete Products in 1987.

He also had senior positions and Directorships in a number of external bodies, including the Ceramic Industries Certification Scheme, British Ceramic Research Limited, the Institute of Ceramics, the National Federation of Clay Industries and the Brick Development Association.

In his later career, from 1994 onwards, he was employed by Ibstock Brick and resigned as a Director in 2014.

The Society and its members pass on our deepest sympathies to his family and friends.

IMS Student Project Awards 2023

Calls are now being made for the 2023 IMS Student Project Awards. Details and Competition Rules together with the Entry Form for the 2023 Award are now available on the website and are also reproduced in this issue of the journal. Any queries should be made to Adrian Bell by email at education@masonry.org.uk

Sustainability e-news from the Masonry Society

The Masonry Society publishes a newsletter on sustainability twice monthly which include a number of papers and articles which may be of interest to our readers. Tools for Improving Performance (February 28, 2023) and Considering the Whole (March 15 2023) are the latest two. The link below provides access to the Masonry Society Website from where the publication may be found. https://masonrysociety.org/tms-sustainability-enews/

Further, TMS launched its Masonry Standards Online Platform in August. The link below provides access to the portal. https://masonrysociety.org/masonry-standards-online

Wienerberger – We Care for a Better Tomorrow

Weinergerger remains committed to a sustainable future despite recent difficult and unstable economic and political conditions, increasing its revenues by 25% over the last year. This growth is as a result of transforming the company into a provider of innovative and sustainable system solutions in the fields of ecological new build and renovation as well as water management.

Even in the challenging 2022 business year, the company adhered to its value-creating growth strategy and remained focused on organic growth through innovation and an increasing share of system solutions in its portfolio, as well as growth through selected value-accretive corporate acquisitions. The latter broadened the company's system solutions competence through the addition of prefabricated wall elements in Austria, increased the exposure to the renovation segment in the field of roofing accessories in Germany, expanded the in-house pipe business in the growth region of South-Eastern Europe, and enlarged the product portfolio by smart system solutions for water management in Norway. In December 2022, by disclosing its intention to take over significant parts of the Terreal Group, Wienerberger announced the biggest step ever in the company's history within the framework of its value-accretive growth strategy. By acquiring the successful European provider of innovative roof and solar solutions, the company will significantly expand its footprint in renovation and repair and evolve into the European pitched-roof expert.

Irrespective of market conditions, Wienerberger has always remained strictly focused on sustainability. In view of climate change and the shortage of skilled labor, smart solutions for resource-saving and energy-efficient building construction and renovation as well as effective water management are continuously gaining in importance. The company is addressing these megatrends by providing solutions that are fit for the future, climate-neutral, and fast and easy to apply, which in turn generates added benefit for its customers.

In the interest of sustainability, the Annual and Sustainability Report is available exclusively as an online document to be viewed via a special interactive micro-site. It provides information on current projects and developments from the World of Wienerberger in the fields of ESG, innovation, digitalization, strategy, and production, alongside presentations of employees from many different fields of business and countries.

https://annualreport.wienerberger.com/2022/

H+H UK Taking a 'reduce, reuse and recycle' approach

H+H UK have adopted policies which will improve the use of resources and reduce waste in addition to minimising energy consumption. The company has installed robust waste management practices through a 'reduce, reuse, and recycle' approach. H+H International has set a target of zero waste to landfill by 2024 however, in the UK this has already been achieved ahead of schedule.

Any waste product from their factories is reused; at their Kent plant waste material is crushed and re-introduced into the production process while at their Yorkshire factory waste goes into another product stream to become part of an aggregate mix. These processes are now ingrained in their manufacturing practices.

The company has also invested in using water efficiently and aims to recycle wastewater wherever possible. For example, at the Yorkshire plant condensate water from the autoclaving process is collected as is all surface water from the yard and all reject water from on-site water filtration systems. In this way an estimated 60% of the company's total water use on site is recycled.

Further, H+H support the principles of a circular economy. At present the company is investigating recycling and re-using waste from construction sites and demolition rubble, which has the potential to be re-used in the production of aircrete.

However, there are currently a number of challenges in recovering and sorting aircrete waste across the wider industry. These must be resolved in order to provide aggregate of a consistent quality and to make the practice of recycling economic for manufacturers or third-party recyclers. In this regard, H+H are supporting efforts to standardise circular processes at an industry-association level and through legislation.

Waste reduction is also being tackled in the transportation and distribution process. For transportation and delivery purposes AAC Blocks produced by H+H are loaded on to wooden pallets. These are recovered, repaired where necessary and reused, a policy endorsed by WRAP (The Waste and Resources Action Programme). This service has diverted 22,000 tonnes of timber from landfill this year alone.

In addition, H+H has minimised the environmental impact of their packaging by using a thinner film. All the packaging material incorporate 30% recycled content.

H+H's latest Sustainability Report can be accessed at www.hplush.com/sustainability-reports

IMS Meetings Update

11th International Masonry Conference July 2026

The 11th International Masonry Conference has been scheduled for July 2026. Details of the location and exact dates will be published in future issues.

THE INTERNATIONAL MASONRY SOCIETY STUDENT PROJECT AWARDS 2023

The International Masonry Society invites submissions of work in which the principal focus of the work is masonry. The award, which is for postgraduate students, is described below.

The **Postgraduate Student Award** would be for a project comprising an MSc dissertation, an equivalent portion of a PhD study or a piece of work (which could include a design study) involving masonry. Exceptional work submitted for this award may additionally be considered for the Arnold Hendry Postgraduate Prize.

Each award will consist of a premium of £150, an International Masonry Society Certificate, and membership of the International Masonry Society for the calendar year following the year of the award.

In exceptional circumstances, more than one award may be made at the discretion of the judges who will also determine the nature of the award.

RULES

1. Submissions must be presented in the form adopted by IMS for the submission of papers for Masonry International (details are attached and are also available at www.masonry.org.uk). Winning submissions will be considered for subsequent publication in Masonry International. The maximum length of submission should not exceed ten pages.
2. Submissions must be made by an academic tutor who is a member of staff of the university or college at which the work was carried out. Normally, the academic tutor will be the principal supervisor of the work.
3. Each submission must consist of a single MSWORD file of the work, accompanied by an electronic copy of the signed entry form and a JPEG photo of the student. The documents should be sent together to Dr Adrian Bell, email: **education@masonry.org.uk**.

4. Submissions for the Postgraduate Student Award must be received by Dr Bell no later than midnight (UK time) on 31 December 2023.
5. All submissions must be in English.
6. Submissions will only be accepted for individual work or for a significant individual contribution to a group project (group work will not be eligible for consideration).
7. The work submitted for an award must have been undertaken as part of a course or research programme completed in 2023. If part of a research programme or group project, the extent of the student input should be stated on a separate sheet attached to the Entry Form, signed by the student and the supervisor. The work must not have been published elsewhere in its current form.
8. Submissions will be assessed by an independent panel of judges appointed by the Council of the International Masonry Society. The decisions of the panel of judges will be final and no correspondence can be entered into concerning the decisions.
9. All submissions will be considered for publication in Masonry International.
10. Winners of an award will be notified via the nominating academic tutors, normally within three months of the submission dates.
11. Results will also be announced in Masonry International.
12. The International Masonry Society reserves the right not to make awards.

Professor John Roberts
The President
January 2023

THE INTERNATIONAL MASONRY SOCIETY STUDENT PROJECT AWARDS 2023

ENTRY FORM

University/College: ……

Academic Tutor: …… e-mail address: ……

Telephone: ……

Address: ……

……

The following student has been nominated to represent my university/college for consideration for the **Postgraduate Award**.

Student name: ……

Course and Year: …… e-mail address: ……

Telephone: ……

Notes

1. An electronic copy of this form, completed in full, must accompany the submission.
2. I accept the conditions which apply to this award.
3. I agree to accept the decision of the judges as final and agree to permit free publication and exhibition of my work by the International Masonry Society.
4. Please include a JPEG photograph of yourself.

Signature (academic tutor): …… Date: ……..

I declare that the report is all my own work.

Signature (student): …… Date: ……..

Instructions for Layout and Format of Award Submissions

Heading in Arial 18 Point Bold Text

T.J. SMITH[(1)], R.W. BROWN[(1)] and A. WHITE[(2)]
[(1)] *Professors, Department of Civil Engineer, Any University, City, County, Post Code and Country*
email@anywhere.co.uk
[(2)] *Centre for Anything, Any University, City, Zip Code and Country, email@anywhere.com*

ABSTRACT
An abstract of around 250 words should be the first section in Arial font size 9pt italic text. The page format is A4 portrait (width 21cm, height 29.7cm). Margins of: top 2cm; bottom 2cm; left 1.5cm; and right 1.5cm are to be used. Two columns of 8.5cm width should be used, with spacing of 0.99cm. Papers are to be prepared using Arial font and text is to be single spaced. The main title, author and affiliations should be size 10pt and centred. The bulk of the text should be size 9pt and fully justified except for section, figure and table titles which should be centred. All papers must be written in English language. All units and abbreviations of dimensions, etc, should conform to SI standards. The Society style is N/mm^2, not MPa. Please ensure N/mm^2 is used, particularly on figures. The full text should not normally exceed 5000 words or typically 12 pages.

This document may serve as a template for the preparation of the papers and authors are advised to copy or type their text directly into this document.

KEYWORDS: authors may list up to 6 keywords in lowercase letters separated by commas.

NOTATIONS
Notations may be listed in the following format:

A	explanation
B	explanation
α	alpha
β	beta

1. INTRODUCTION

Each section should be numbered with the uppercase title centred in the column. Subheadings should be in the format below.

New paragraphs within the text should be indicated by indenting at 0.25cm.

1.1 Heading to be inserted
Headings for subsections should be left justified, in bold and all lower case.

1.2 Heading to be inserted
Headings for subsections should be left justified, in bold and all lower case. If a sub-subheading is required, the format below should be followed.

1.2.1 Heading to be inserted
Sub-subheading should be left justified and all lower case.

1.2.2 Heading to be inserted
Sub-subheading should be left justified and all lower case. If yet another level of sub-heading is required, the format below should be followed.

1.2.2.1 Heading to be inserted
These headings should be italic, left justified and all lower case.

2. EQUATIONS

Equations should be numbered with the equation appearing on the left and the number, in brackets, appearing on the right with a line space above and below the equation. All equations should be referenced in the text. For example, see Equation (1) below:

$$\gamma_E \cdot E \leq \frac{R}{\gamma_R} \qquad (1)$$

3. FIGURES AND TABLES

3.1 Figures
All figures appearing in the paper must be referred to in the text. Figures may be photographs, graphs or drawings but must be greyscale with no colour and should be placed at the end of the paper. Figure captions should be bold, centred, and placed below the figure. As an example see Figure 1 at the end of this template.

3.2 Tables
All tables appearing in the paper must be referred to in the text. Tables should have no colour or shading and be placed at the end of the paper. Table captions should be bold, centred, and placed above the table. As an example see Table 1 at the end of this template.

4. DOCUMENT FORMAT

Papers are to be submitted electronically in Microsoft Word in a format compatible with previous versions of the software. Student Awards entry forms and papers should be sent to Dr Adrian Bell, email: **education@masonry.org.uk**.

ACKNOWLEDGEMENTS
Acknowledgements may be made. The title should be without numbering, in upper case, bold and left justified.

REFERENCES
References should be numbered in the order they appear in the text (i.e. NOT according to their alphabetical order) and should appear, fully justified, in the last section of the paper as in the example below [1]. The authors name should be uppercase (surname followed by initial(s)) with the title of the paper in lowercase. If it is a book, the title should be italic and followed by the publisher and place of publication. If the correct abbreviation of a journal is unknown, it should be quoted in full. The volume number should be in bold, with the issue number in parentheses. This is followed by the page number(s) and date. Private communications, unpublished work or restricted publications should not be quoted, but may be mentioned in the text. The Harvard method of referencing is also permitted as an alternative.

1. SMITH, T.J., BROWN, R.W. and WHITE, A. Title of the Paper, Masonry International **25**, (1), 8, 2012.
2. TAYLOR, H.F.W., Chemistry of Cement, 2nd Ed, Thomas Telford 1997 pp231-235

Figure 1 Title of figure in lowercase, Arial font size 9pt, bold and centred

Table 1
Title of table in lowercase Arial font size 9pt, bold and centred

No.	Model	Titles in bold and centred in the cell		
		a	b	c
1	CC10	21.0	5.6	8.4
2	UY6	18.3	9.1*	4.4
3	HG7	14.5	8.5	7.2
4	JP4	16.6	5.8	6.1
5	MC14	Not applicable		

* Notes should be placed below the table

Prediction of the Seismic Behaviour of an Iconic Masonry Pagoda in China

P.X. WANG[1], G. MILANI[1], S.C. LI[2], [3]
[1] *Politecnico di Milano, Department of Architecture Built Environment and Construction Engineering, Piazza Leonardo da Vinci, 32, 20133, Milan, Italy*
[2] *School of Architectural Science and Engineering, Yangzhou University, 225127, China.*
[3] *Jiangsu Huajian Construction Co., LTD, 225002, China.*
peixuan.wang@polimi.it, gabriele.milani@polimi.it, lisc@yzu.edu.cn

ABSTRACT
Relevant damage to historical masonry structures mainly comes from earthquakes. This paper focuses on the prediction of the seismic behaviour of a masonry pagoda in China using non-linear static and dynamic analyses, whose results are then compared with a more straightforward procedure, represented by a limit analysis with pre-assigned failure mechanisms. Pushover and non-linear dynamic numerical simulations are carried out in Abaqus which can satisfactorily predict the generation and development of earthquake-induced damage in masonry structures. At the same time, manual limit analysis is an important tool for common practitioners to assess seismic vulnerability quickly and effectively. Together they represent, therefore, an excellent protocol to follow. This research applies the above methods to an ancient iconic Chinese masonry pagoda – namely the Zhongjiang South Pagoda, located in the Sichuan province PRC. It has an octagonal cross-section containing a central room and a staircase that spirals upwards in a clockwise direction. After the 2008 Wenchuan Earthquake, Zhongjiang South Pagoda suffered serious damage. Surveys have shown that seismic loads caused a bottom-up crack in the middle part of the pagoda and almost activated the collapse by rocking on an inclined plane through the bottom 2-3 floors. The numerical results obtained are in general agreement with what occurred in reality and provide positive recommendations for the protection and repair of ancient masonry pagodas and towers in general.

KEYWORDS: seismic vulnerability; masonry pagoda; numerical simulations; limit analysis; collapse mechanism

1. INTRODUCTION

Chinese historical architecture, stemming from one of the most important ancient civilizations, is a precious heritage that must be preserved. Such architecture includes masonry pagodas, unique and important historical structures deserving of preservation. Pagodas are widely dispersed across the Far East, but they are mainly concentrated in China. Records show that more than 10,000 pagodas have been built and roughly one-third still stand [1]. From a structural point of view, they are massive cantilevers characterized by materials with low tensile and shear strength, and so not able to resist seismic events, even ones of moderate intensity [2]. However, China is prone to severe earthquakes and damage and collapses observed in masonry pagodas are mostly a consequence of them. For example, the pagoda of Famen temple in Shaanxi collapsed because it was not repaired and strengthened after a strong initial shock [3]. The Wenchuan Earthquake on May 12, 2008 also devastated masonry structures in the Sichuan region, including pagodas. However, current knowledge of the behaviour of pagodas under horizontal loads stills needs further improvement. Further, immediately after a strong earthquake, it is of paramount importance to identify the damaged parts in a timely and efficient manner, predict damage development, and propose remedial protection measures.

Xi'an University of Architecture and Technology, Southeast University, Yangzhou University in China, Politecnico di Milano in Italy, Seoul National University in South Korea, the University of Minho in Portugal, and many other renowned university research centres [4-9] have made great efforts in the past few decades to predict the seismic behaviour, to identify the dynamic characteristics, and to evaluate the reliability of the calculation methods currently used in assessing the effects of earthquake on masonry structures. Recent studies have shown that under the application of horizontal loads, pagodas may collapse due to well-defined failure mechanisms being triggered. These mechanisms have been classified. In [10,11], for instance, the upper bound (kinematic) theorem of limit analysis has been proposed to quickly evaluate the seismic vulnerability of masonry towers, which exhibit geometries and materials similar with pagodas. Based on this, five main collapse mechanisms have been identified, namely: 1) vertical splitting in two parts, 2) base rocking, 3) overturning with diagonal cracks ("a Heyman" mechanism), 4) a combination of splitting and diagonal overturning, and 5) base sliding [10-12]. Of these, vertical cracking in the middle part of the element seems to be the most common damage observed. This manual limit analysis method has a short calculation time, low computational cost, and is easy to understand. However, it can only provide the collapse multiplier under a given pre-assigned mechanism. This approach seems suitable for pagodas, which are expected to behave in a similar way, structurally.

However, no information is given on the displacements at collapse, and the assumption of pre-assigned failure mechanisms could lead to an overestimation of the load-carrying capacity.

Non-linear Finite Element analyses are currently a common approach for simulating damage propagation in masonry towers and pagodas subjected to earthquake loads. Commercial Finite element software, such as Abaqus, Ansys and Adina have been widely used in the recent past, and with their comprehensive libraries of fragile material models, they can provide a deep level of insight into the actual behaviour of masonry structures in general, far beyond the elastic limit [13-23]. By taking the necessary measures to enhance the convergence of calculations and, if used by experienced technicians, they could provide valuable information on the expected behaviour of masonry pagodas. However, they are complex to run for someone not an expert in the field, because they require the user to set a large number of mechanical and numerical parameters.

Considering the advantages and disadvantages of the above-mentioned finite element approaches and manual limit analysis methods, this paper applies a mixed set of rules based on both complex FE computations and direct limit analysis aimed at the protection of masonry pagodas in general, selecting the Zhongjiang south pagoda as a case study. In particular, both pushover and non-linear dynamic analyses are carried out, and the results are compared with those provided by a simple manual limit analysis. The purpose is to accurately assess the damaged parts of the masonry pagoda after a possible earthquake similar to that which occurred in 2008, reproducing the crack patterns developed and predicting the ultimate seismic acceleration. Comparing the results obtained using different methods could be extremely important in implementing a protection plan based on the reducing seismic vulnerability, as conceded by many other similar case studies.

2. HISTORY of ZHONGJIANG SOUTH PAGODA

2.1 Background of Zhongjiang South Pagoda

Zhongjiang South Pagoda is located in Zhongjiang City, Sichuan Province (Figure 1). It was built in the Wanli period of the Ming Dynasty and is a provincial-level cultural relic protection unit. The lower level of the pagoda opens to the north, and the horizontal cross section is octagonal, with a side length of about 8 meters. Its height is about 30.2 meters. There are nine floors inside the pagoda, and each floor can be visited. There is also a central room for storing scriptures and scrolls. The central room is in the north part of the pagoda body. Doors facing in different directions are present on the facades of each floor, and windows may be opened on those facades without doors. From the viewpoint of the façade, the Zhongjiang South Pagoda reduces in section as one moves upwards, regularly over the first seven floors, then more rapidly over the last two [2].

On May 12, 2008, a magnitude 8.0 earthquake occurred in Wenchuan, Sichuan, China. Zhongjiang South Pagoda is about 114km from the epicenter of Yingxiu city (Figure 2) and was seriously damaged. The pagoda body cracked, the eaves collapsed, and the pagoda spire fell. From 2009, as a consequence of such events, the Chinese government organized a series of targeted restoration works to effectively protect the traditional architectural heritage of the country [24].

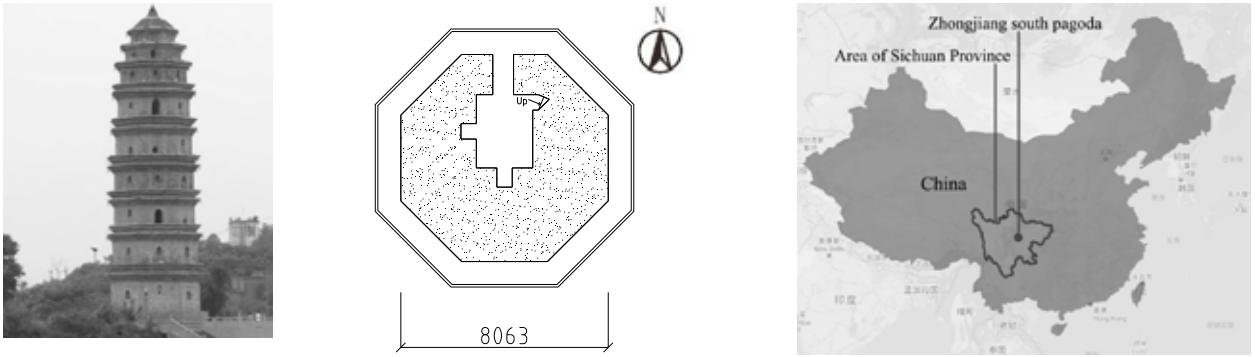

(a) Current situation **(b) Plan of the first floor** **(c) Location**

Figure 1 Zhongjiang south pagoda [2]

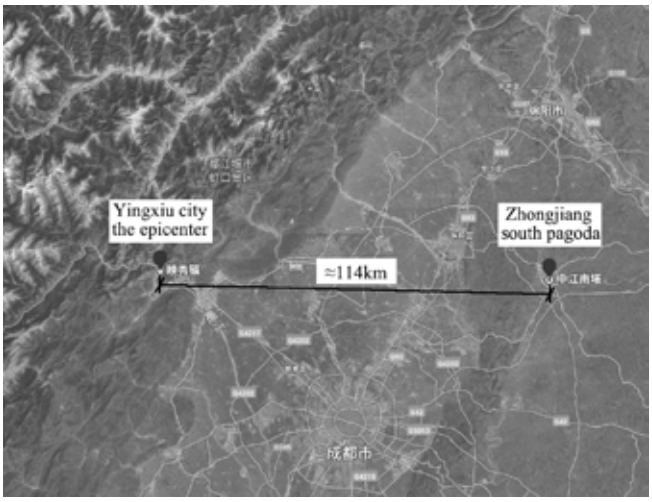

Figure 2 The distance between Zhongjiang south pagoda and the epicenter of the Wenchuan earthquake

3. NUMERICAL SIMULATIONS

To analyse the seismic vulnerability of the pagoda and study how damage could spread within the structure, finite element analysis has been used. Several pushover analyses and two non-linear dynamic numerical simulations have been performed using the commercial software Abaqus.

A research team of Yangzhou University and Shaanxi Architectural Design and Research Institute conducted on-site tests on the brick materials of each layer of the Zhongjiang South Pagoda [2,24-27]. The strength of the mortar was measured by the pouring method. The design value for masonry compressive strength was determined by referring to the specification "Code for Design of Masonry Structures" GB 5003-2001 [28]. Based on the on-site test results and considering the degraded characteristics of this type of ancient masonry as recorded in the literature, in this paper, the mechanical properties used are summarized in Table 1. Particularly low values for the tensile strength and the fracture energy in tension were chosen, to reproduce as closely as possible the near zero-tension material hypothesis.

Masonry is composed of bricks and mortar, each component having relatively regular textures. Globally, though, the behaviour is expected to be orthotropic, and the crack pattern could be influenced by such a feature. However, no numerical models are available in Abaqus to deal with such features. Nevertheless, when the well-known Concrete Damage Plasticity model CDP of Abaqus, was suitably adapted via the set parameters, it proved to be reasonably accurate in the prediction of the global behaviour of such structures even in the absence of orthotropy. Therefore, pushover and non-linear dynamic analyses are carried out utilising the adapted CDP. The parameters that specifically refer to CDP are summarized in Table 2 and have been gleaned from a number of references [29-31]. To avoid spurious additional-strength characterized by unrealistic hardening, low values for the viscosity parameter (0.0001) are assumed, a choice that ensures the accuracy of the simulation results and prevents overestimations of the capacity.

3.1 Modal analysis

Based on previously conducted sensitivity analyses, the discretization of the pagoda is made using 58777 solid linear elements (Figure 3(a)) to ensure calculation accuracy and save calculation time. A preliminary modal analysis shows that the first (along X) and the second (along Y) vibrational modes of the structure are typical for a cantilever (Figure 3), with periods of about 0.59g, corresponding to accelerations located in the descending branch of the spectrum.

Table 1
Material properties of Zhongjiang south pagoda's masonry

Specific weight	Young's Modulus	Poisson's ratio
18kN/m^3	1600MPa	0.25
Compression Strength	**Tensile Strength**	**Tensile Fracture Energy**
1.5MPa	0.05MPa	0.007N/mm

Table 2
Parameters of CDP model in abaqus

Dilatancy Angle	Eccentricity	*fb0/fc0*	Viscosity Parameter
10°	0.1	1.16	0.0001
fb0: initial equibiaxial compressive yield stress. fc0: initial uniaxial compressive yield stress.			

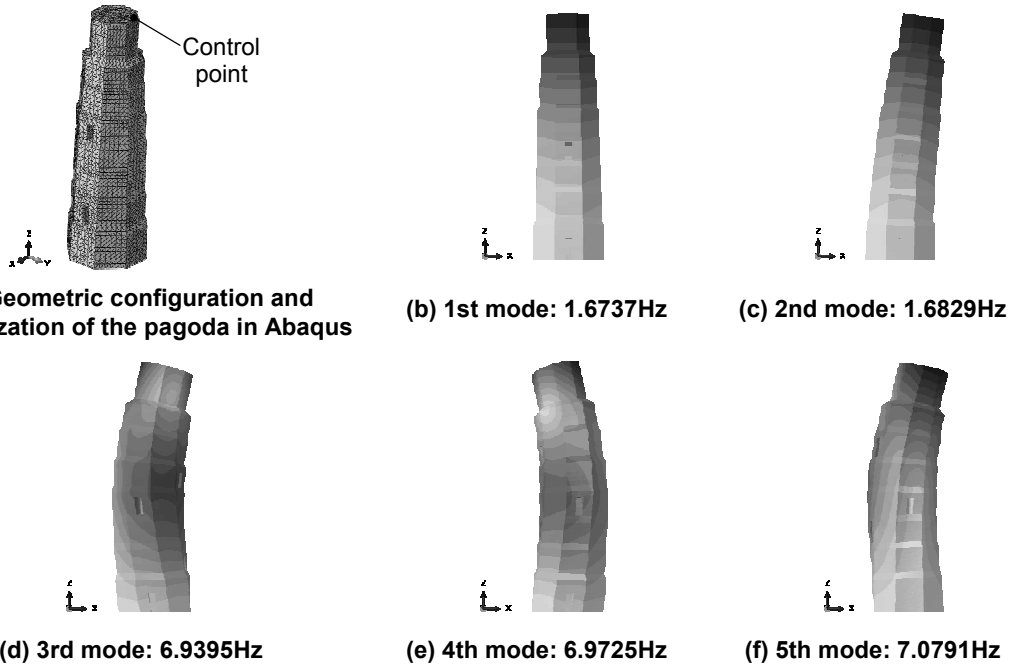

(a) Geometric configuration and discretization of the pagoda in Abaqus

(b) 1st mode: 1.6737Hz

(c) 2nd mode: 1.6829Hz

(d) 3rd mode: 6.9395Hz

(e) 4th mode: 6.9725Hz

(f) 5th mode: 7.0791Hz

Figure 3 Different vibration modes

3.2 Pushover analyses

The pushover analysis method is a representation of a seismic analysis obtained by applying statically and monotonically increasing horizontal loads to a structure, mainly to study the nonlinear performance when it enters the plastic state under the action of an earthquake. According to the obtained capacity curve (shear force at the base of the structure vs displacement at the top for a tower), the seismic capacity of the structure is evaluated. Pushover is an approximate approach that converts dynamic problems into static ones. In this research, pushover analyses are conducted along four directions, namely X+, X−, Y+, and Y−, and applying two kinds of load distributions, G1 and G2. In G1, the primary distribution of forces is directly proportional to the mass and increases linearly with the structure's height. This distribution is commonly called the "inverted triangle distribution" in the Italian code and various other codes of practice. G2 load distribution is also proportional to the mass but remains constant throughout the structure's height [31]. Although the masonry pagoda with its octagonal plane is almost symmetric, each façade has different openings, and the inner central rooms are close to the northern part. Therefore, slight differences in the simulation results were expected for the different cases, which are worth investigating. Investigations are based on the capacity curves in terms of a_g/g (normalized shear at the base over the gravity acceleration), displacement of a node located at the top as shown in the paper, and a discussion is also made looking at the resulting damage found at failure.

The results show that the damage of the pagoda under G1 and G2 loading conditions in the same direction is similar. In Figures 4-11, no matter the direction, the seismic loads act in, the damage is mainly suggestive of an overturning at the base with diagonal cracks, with damage spreading from the first to the third floors. The elastic behaviour is lost in a range between 2.5mm and 3mm of top displacement.

The crack pattern found, however, does not fit that observed with sufficient accuracy. Intuitively, the vertical splitting crack occurring in reality, should also be seen in the simulations because the internal central rooms are mainly located near the northern part of the pagoda; the external walls are therefore less thick, and their tangential shear strength could be insufficient to prevent the diffusion of shear cracks. A possible explanation of such misalignment with experimental evidence could be due to a too-rough discretization of the structure. It should be pointed out here that surveys have also shown that a crack develops longitudinally on the north façade. The crack first appears on the first floor and gradually extends upwards along the openings. This is mainly because the thickness of the wall in this part is small, and hence the bearing capacity is lower. The aforementioned damage pattern could be in agreement with that found numerically in the non-linear static analyses.

Figure 12 shows all the capacity curves plotted on the same graph, and it is possible to see that the G2 loading condition exhibits a higher ultimate a_g/g of around 0.225g, whilst - and as expected - the G1 distribution is characterized by a lower ultimate load of around 0.17g. In the present pagoda, although the central rooms are distributed close to the north side of the pagoda body, the capacity curves under seismic loads along the positive X and negative Y directions are not very different. Pushover results, at least globally, seem not particularly sensitive to such geometric features.

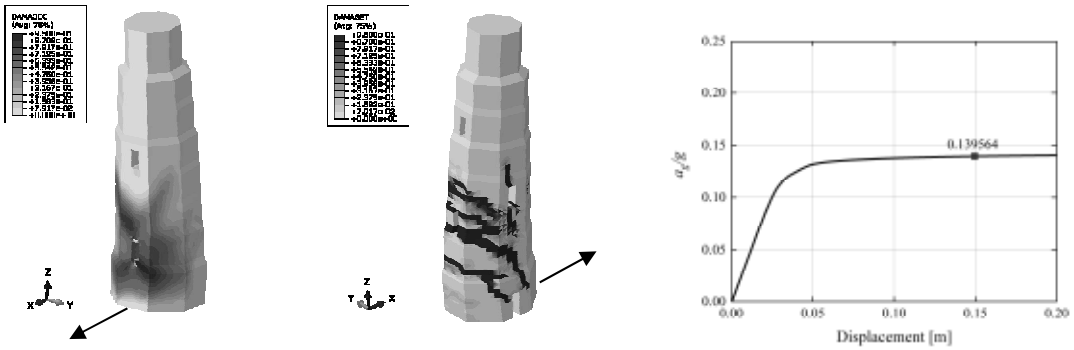

(a) Compressive damage **(b) Tensile damage** **(c) Capacity curve**

Figure 4 Results of pushover analysis in X+ direction with G1 load

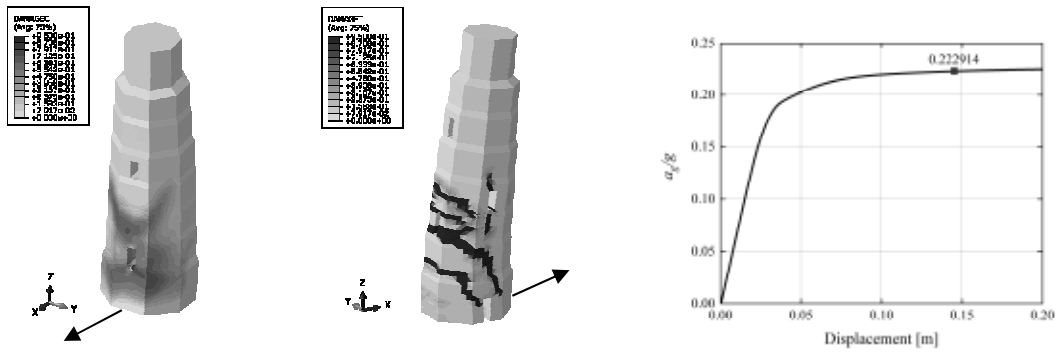

(a) Compressive damage **(b) Tensile damage** **(c) Capacity curve**

Figure 5 Results of pushover analysis in X+ direction with G2 load

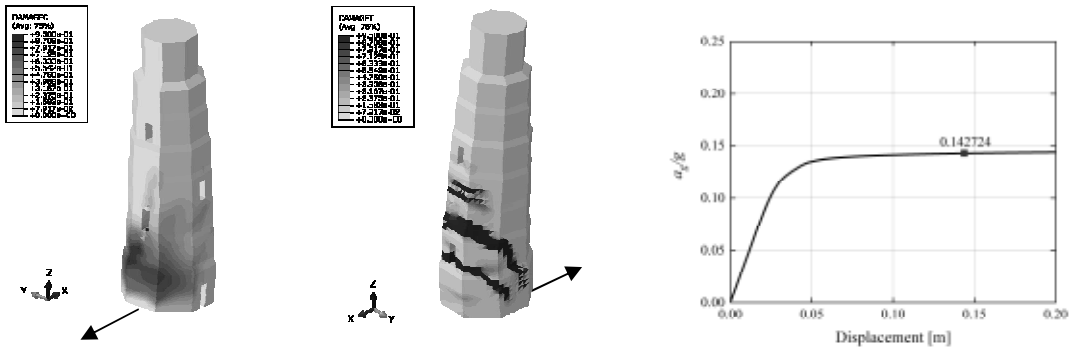

(a) Compressive damage **(b) Tensile damage** **(c) Capacity curve**

Figure 6 Results of pushover analysis in X- direction with G1 load

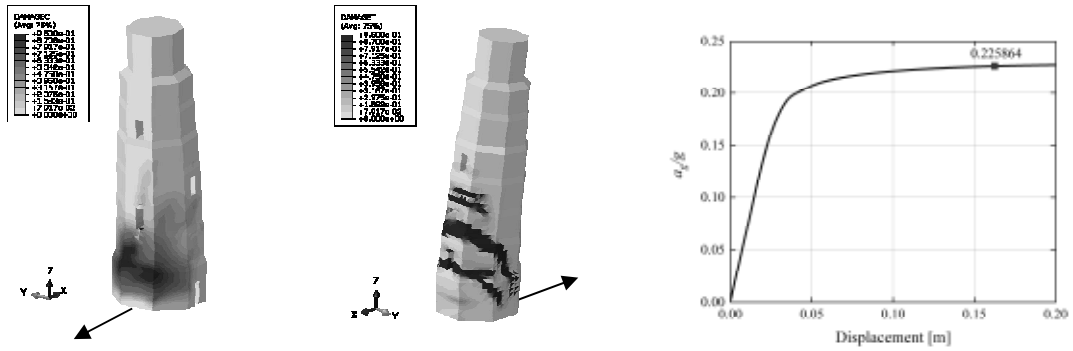

(a) Compressive damage **(b) Tensile damage** **(c) Capacity curve**

Figure 7 Results of pushover analysis in X- direction with G2 load

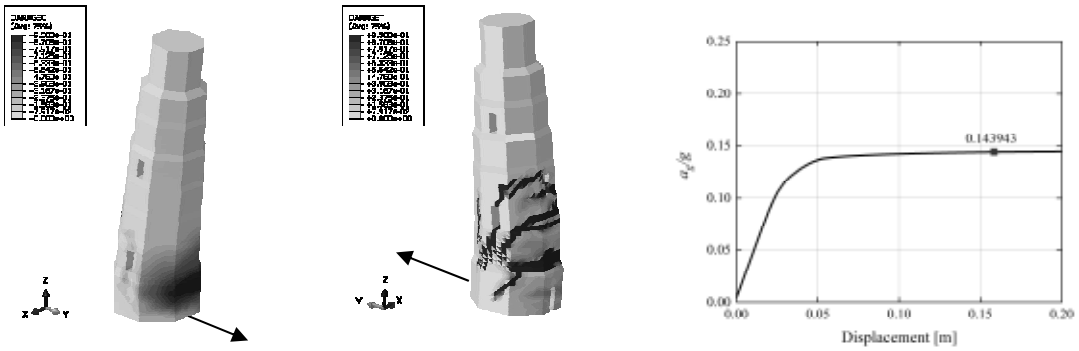

(a) Compressive damage **(b) Tensile damage** **(c) Capacity curve**

Figure 8 Results of pushover analysis in Y+ direction with G1 load

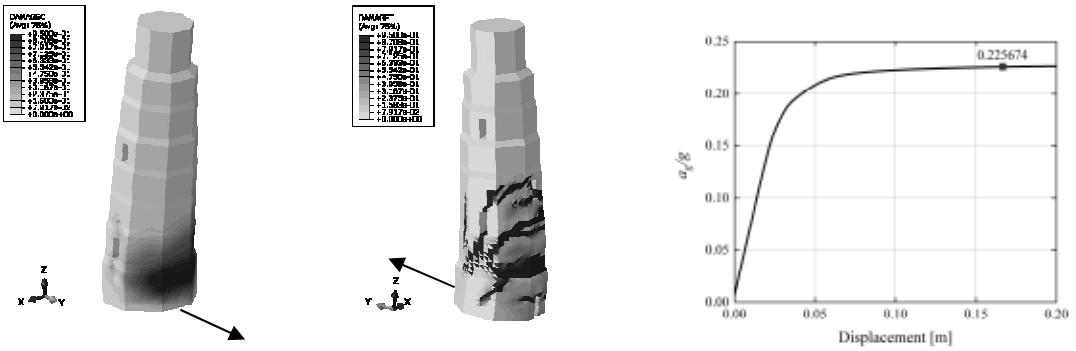

(a) Compressive damage **(b) Tensile damage** **(c) Capacity curve**

Figure 9 Results of pushover analysis in Y+ direction with G2 load

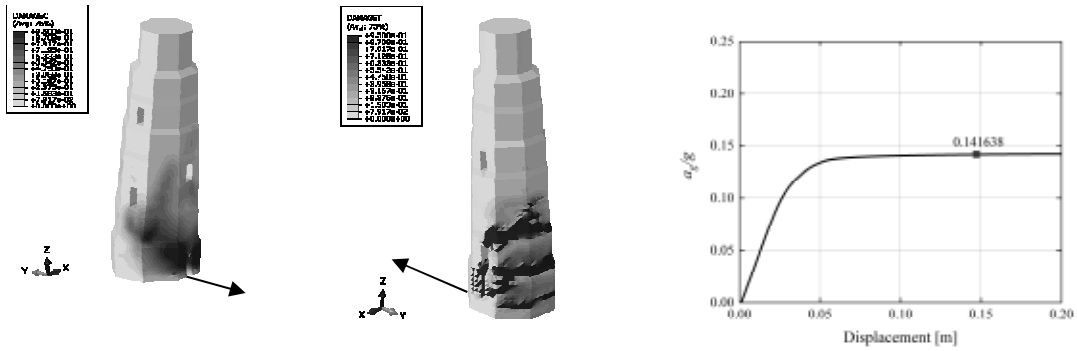

(a) Compressive damage **(b) Tensile damage** **(c) Capacity curve**

Figure 10 Results of pushover analysis in Y- direction with G1 load

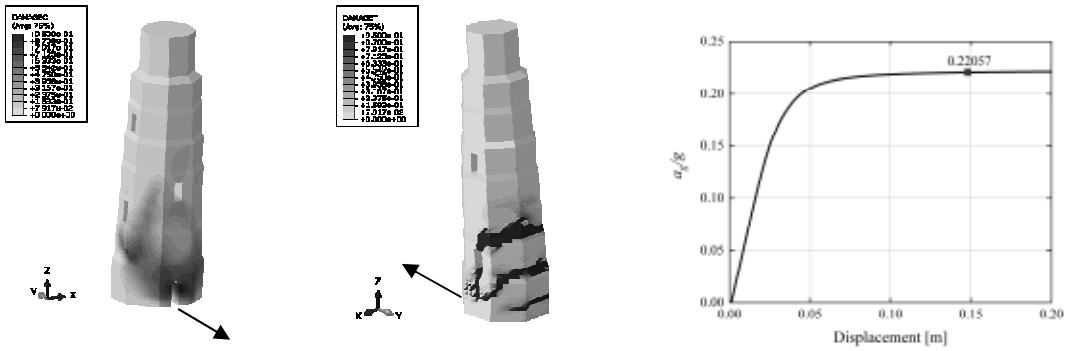

(a) Compressive damage **(b) Tensile damage** **(c) Capacity curve**

Figure 11 Results of pushover analysis in Y- direction with G2 load

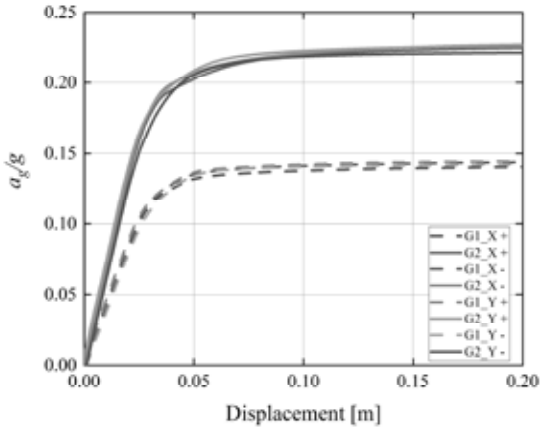

Figure 12 Capacity curves of Zhongjiang south pagoda

3.3 Non-linear dynamic analysis (NLDA)

To have further insight into the prediction of the actual crack pattern that can develop during a seismic event, two non-linear dynamic analyses were also performed. To define the seismic input for the NLDA, an accelerogram has to be selected. In this work, an artificial accelerogram is generated (spectrum-compatible accelerogram) using the spectrum provided for that region by the Chinese seismic code. There is also a real accelerogram available, which is the ground motion recorded during the 2008 earthquake by Wolong Wenchuan station, but this station is not particularly near the earthquake epicenter, a feature that could considerably reduce the peaks of acceleration that actually could act on the pagoda and could therefore, in principle not accurately predict the crack pattern developed. It is therefore considered unsuitable for the present case study, and this is the reason why the spectrum-compatible accelerogram of Figure 13 is used. It has been computed from the elastic spectrum provided by the Chinese Building Code [32] by using the SeismoArtif software [33]. Before the implementation, the artificial accelerogram was filtered by the SeismoSignal software [34] to reduce anomalous peaks and hence strengthen the computational efficiency. Furthermore, the peak acceleration has been scaled to 0.14g, in accordance with the collapse acceleration found in pushover analyses with a G1 distribution.

A cross-check with the results obtained with pushover analyses suggests that such an accelerogram would be a good one to induce the necessary damage to the pagoda and be able to initiate a collapse mechanism. A classic damping of 5% was assumed.

Two non-linear dynamic analyses are performed along the X and Y directions respectively, applying the acceleration history at the base. As can be seen from Figure 13, when applying the accelerogram along X, damage first appears at the openings on the third floor of the north and south facades within about 4 s. Subsequently, the crack extends upwards and downwards in the vertical direction. After 5.8s, the crack reaches the sixth floor and develops further in a Y-shaped pattern towards the east and west directions. It is worth noting that there is also a vertical crack that appears at about 5.5s on the east and west facades. After around 8s, the masonry pagoda can no longer bear the earthquake loads, the number of cracks in the pagoda increases, and the masonry structure overturns and collapses.

When the accelerogram is applied along the Y direction (Figure 14), the vertical crack appears at around 3.4s, along the center line of the east and west facades. When the crack reaches the sixth floor, it alters, growing obliquely towards the north direction. After 6s, the cracks spreads above the sixth floor in the north and south directions and upwards in a Y-shape. Up until 13.3s, the damage spreads further, simulating the entire seismic event.

Comparing the collapse mechanisms provided by pushover and non-linear dynamic analyses, there are certain similarities and differences. The horizontal load exerted by pushover on the pagoda is obviously unidirectional, and the main reason for collapse seems to be the activation of an overturning effect along the direction of the applied load resulting in the formation of inclined cracks at the lower 2-3 floors. Simultaneously, a vertical crack spreads up the middle of the pagoda, but it does not extend to the top. The seismic load exerted on the pagoda in dynamic simulations shows that although the structure still has the risk of overturning along the transverse section of the bottom layer, the most important damage is the crack developing in the middle that runs through the pagoda body from bottom to the top.

Setting a control point (Figure 3(a)) at the center of the top of the tower and observing the time-displacement history (Figure 15), some interesting observations can be made. First, the displacements of the pagoda in the X and Y directions are very similar up to 8s because there is a high degree of symmetry. The maximum displacement occurs within 6-8s and reaches about 16cm-18cm. Also, between 6 and 8s, the vertical crack develops and stabilizes in both cases. The difference is that when the seismic load is applied along the X direction, the crack starts widening, the collapse mechanism activates completely, and the tower collapses during the seismic event. On the contrary, the final residual displacement for the Y direction is close to zero, which indicates that the tower has developed a crack pattern completely compatible with the collapse but still has some residual capacity and remains in equilibrium under vertical loads. The application of after-shock accelerograms of moderate intensity is expected to cause the structure to collapse.

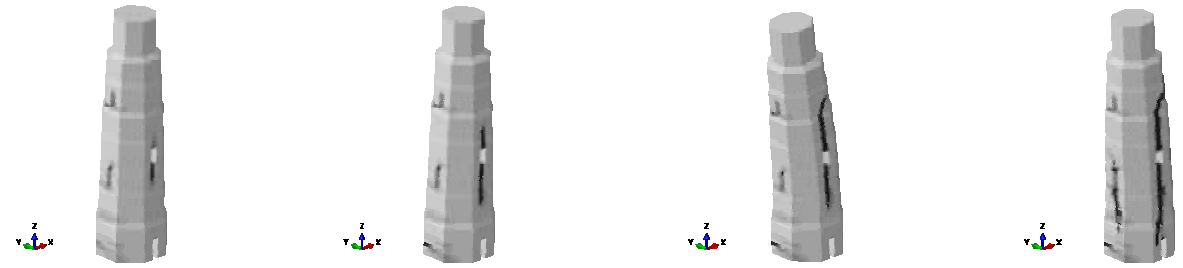

Point 1: 3.967s **Point 2: 4.500s** **Point 3: 4.805s** **Point 4: 5.448s**

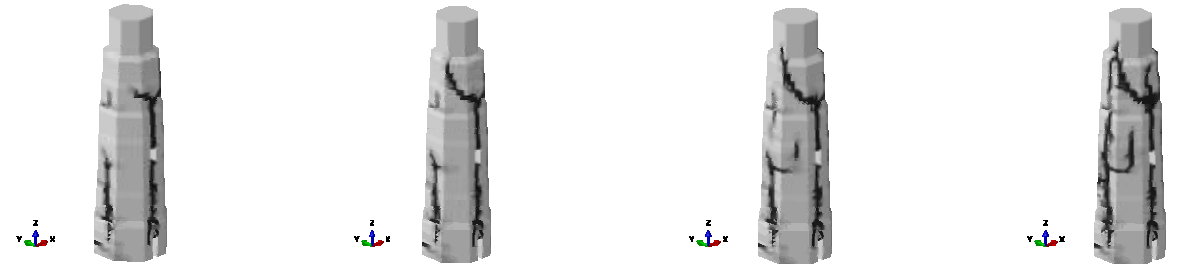

Point 5: 5.773s **Point 6: 6.457s** **Point 7: 8.102s** **Point 8: 8.313s**

(a) Tensile damage

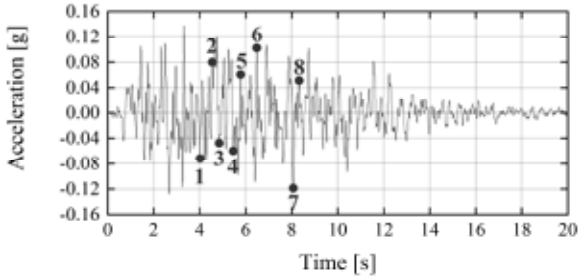

(b) Accelerogram

Figure 13 Results of non-linear dynamic analysis in X direction

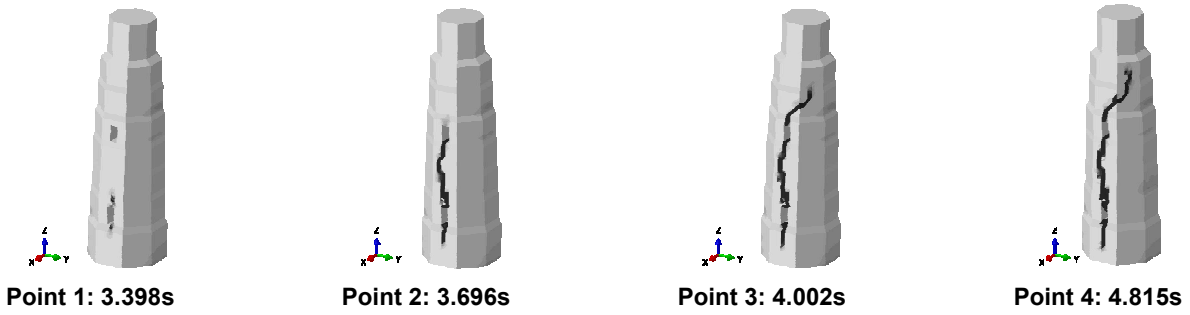

Point 1: 3.398s | Point 2: 3.696s | Point 3: 4.002s | Point 4: 4.815s

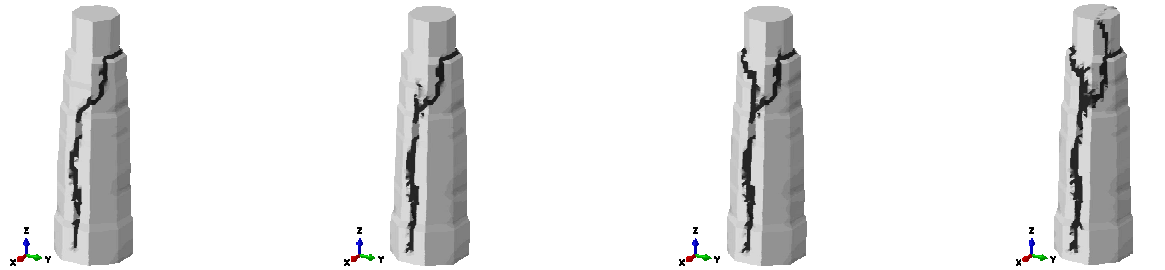

Point 5: 5.071s | Point 6: 5.738s | Point 7: 6.027s | Point 8: 13.250s

(a) Tensile damage

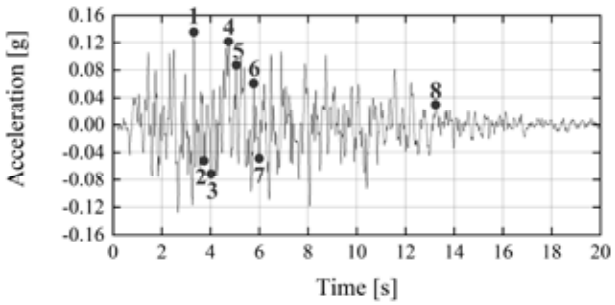

(b) Accelerogram

Figure 14 Results of non-linear dynamic analysis in Y direction

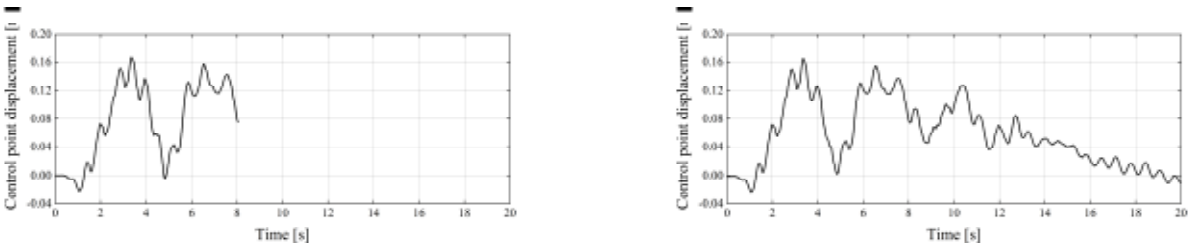

(a) X direction **(b) Y direction**

Figure 15 Displacement time-history for NLDAs under the spectrum-compatible accelerogram

4. MANUAL LIMIT ANALYSIS

A manual limit analysis along the X+ direction with G1 load distribution was also performed [10-12], in which five pre-established collapse mechanisms are assumed and summarized in Figure 16. The failure planes of Mechanism n.3 and n.4 are taken with inclination angles equal to 30°, 45°, and 60° with respect to the horizontal direction. In mechanism n.5, a friction angle of 30° is assumed (Figure 16).

Table 3 summarizes the results in terms of collapse accelerations obtained using manual limit analysis. Vertical splitting into two parts (mechanism n.1) exhibits the smallest collapse acceleration, which is 0.135g., meaning it is the mechanism most likely to occur, at least in a limit analysis prediction; considering both the rough simplifications of the approach used and the damages observed after the earthquake, this is valuable information for a possible future implementation of a strengthening procedure to reduce the vulnerability. However, the collapse

acceleration of mechanism n.4 is also close to the minimum one, a feature that tends to justify the predictions of both pushover and non-linear dynamic analyses. Discrepancies may be caused by the different material models and parameters used by the two analysis methods, which do not have anything in common. In any case, considering again mechanism n.4, the acceleration at collapse for an angle equal to 30° for the rocking plane is equal to 0.168g, which overestimates the pushover prediction by 13.5%, a result that from an engineering standpoint appears fully acceptable.

5. CONCLUSIONS

In this paper, an iconic masonry pagoda (Zhongjiang South Pagoda) was selected as a case study to predict its seismic vulnerability using different computational methodologies, namely non-linear static, non-linear dynamic, and limit analyses. Despite the very different material models used in the analyses and the approximations introduced, all results converge to a well-defined value of collapse acceleration and a failure mechanism characterized by the spreading of a big sub-vertical crack. The presence of secondary rocking on an inclined plane near the base is also predicted by all the methods used.

The authors' future research directions will focus on the application of the protocol proposed to more masonry pagodas with different geometries and architectural features to consolidate the reliability of the approach proposed. A further development will be to remove the restriction of manual limit analysis made at the beginning, namely the apriori assumption of a certain mechanism active, for instance, by a discretization into Finite Elements or Distinct Elements of the geometry [35-39]

ACKNOWLEDGEMENTS

The work has been supported by the Chinese Scholarship Council CSC (award to Peixuan Wang for 4 years of Ph.D. study abroad at the Technical University of Milan, Italy).

Gabriele Milani would like to thank the Technical University of Milan Institution for making partially possible the research and for awarding him a sabbatical period for research in collaboration with Yangzhou University PRC.

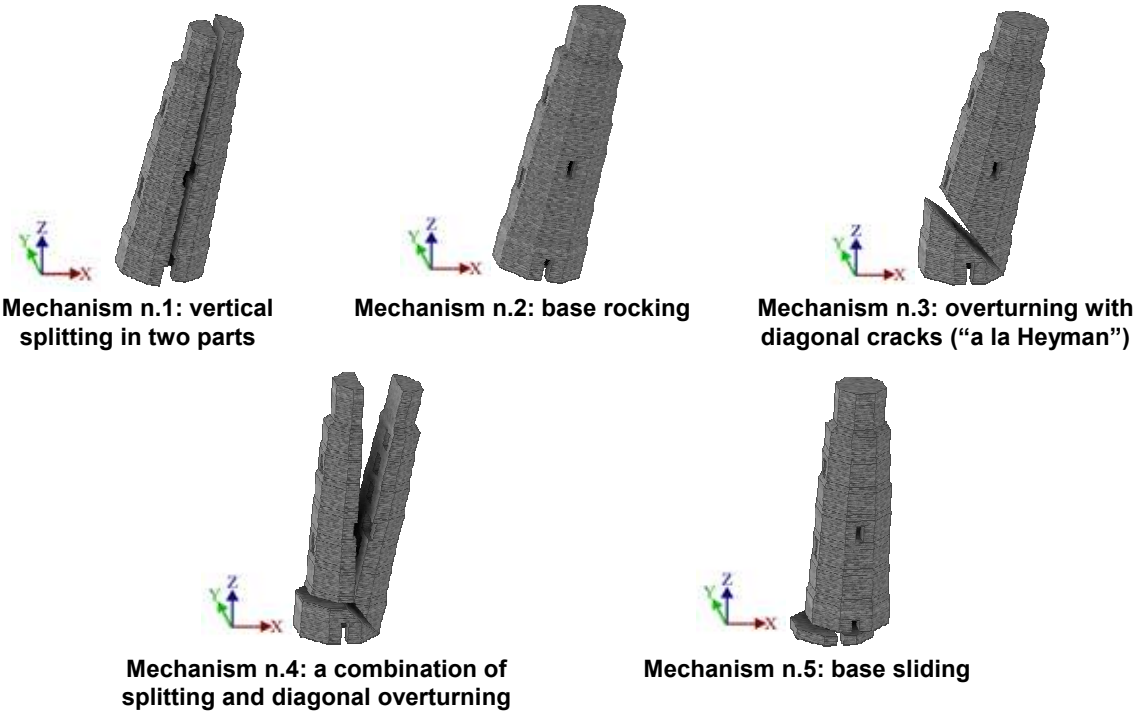

Figure 16 Manual limit analysis of Zhongjiang south pagoda in X+ (0°) direction with G1 load

Table 3
Manual limit analysis of Zhongjiang south pagoda in X+ (0°) direction with G1 load

Mechanism	Inclination Angle [°]	Collapse multiplier of Zhongjiang south pagoda [g]
#1	/	0.135
#2	/	0.269
#3	30	0.236
	45	0.219
	60	0.200
#4	30	0.168
	45	0.178
	60	0.210
#5	/	0.577

REFERENCES

1. SHENG, Z.G. Study on the Mechanical Properties, Appraisal, and Reinforcement Methods of Ancient Masonry Pagodas, Xi'an University of Architecture and Technology in China, Master thesis, 2005. [In Chinese]
2. HU, Y.X. Earthquake Engineering, Beijing: Earthquake Publishing House, 2006. [In Chinese]
3. LUO, Z.W. Chinese Ancient Pagoda, Beijing: China Youth Publishing House, 1985. [In Chinese]
4. LING, J.A. Combination Rectification Method to Straighten Lanzhou White Pagoda, Construction Technology, 2, 1999. [In Chinese]
5. CHEN, P., YAO, Q.D., and ZHAO, D. Study on Seismic Capability of Xi'an Dayan Pagoda, Journal of Building Structures, 2, 1999. [In Chinese]
6. CAO, S.Y., QIU, H.X., and LI, Y.P. Systematic Method and Application of Reliability Diagnosis of Ancient Pagoda Structure, Special Structure, 1999. [In Chinese]
7. QIU, H.X. A Systems Approach to Structural Damage, Dongnan University, Ph.D. thesis, 2000. [In Chinese]
8. KIM, J., and RYU, H. Seismic test of a full-seale model of a five-storey stone pagoda, Earthquake Engineering and Structural Dynamics **32**, 2003 pp731-750.
9. VASCONCELOS, G. Experimental Investigations on the Mechanics of Stone Masonry, the University of Minho for the Degree of Doctor of Civil Engineering, 2005.
10. SARHOSIS, V., MILANI, G., and FORMISANO, A., and FABBROCINO F. Evaluation of Different Approaches for the Estimation of the Seismic Vulnerability of Masonry Towers, Springer Netherlands, **16**, 2018.
11. MILANI, G. Fast Vulnerability Evaluation of Masonry Towers by Means of an Interactive and Adaptive 3D Kinematic Limit Analysis with Pre-assigned Failure Mechanisms, International Journal of Architectural Heritage, **13**, 2019, pp941–62.
12. ACITO, M., CHESI, C., MILANI, G., and TORRI, S. Collapse analysis of the Clock and Fortified Towers of Finale Emilia, Italy, after the 2012 Emilia Romagna Seismic Sequence: Lesson Learned and Reconstruction Hypotheses, Construction and Building Materials, **115**, 2016, pp193–213.
13. ZHU, B.L, et al. Finite Element Elastoplastic Analysis of "Mixed System" Medium-sized Masonry Block Walls, Journal of Tongji University, 01, 1994. [In Chinese]
14. FORMICA, G., SANSALONE, V., and CASCIARO, R. A Mixed Solution Strategy for the Nonlinear Analysis of Brick Masonry Walls, Computer Methods in Applied Mechanics and Engineering, **191,** (51–52), 2002, pp5847–5876.
15. MIAO, J.J., et al. Numerical Simulation of Collapse Response of Masonry Structure under Earthquake, Journal of Civil Engineering, 09, 2005. [In Chinese]
16. PENG, B. Graphic Simulation Technology of Collapse Response of Masonry Structure, Journal of Tongji University, 10, 2004.
17. WANG, S.H., TANG, C.A., et al. Numerical model and simulation analysis of cracking process of masonry. Engineering Mechanics, **22**, (02), 2005, pp56–61. [In Chinese]
18. SAMARASINGHE, W., PAGE, A.W., and HENDRY, A.W. Behaviour of Brick Masonry Shear Wall, The Structure Engineering, **59B**, (03), 1981, pp42–48.
19. YUE, J.Y., and WANG, Y.T. Research on the Dynamic Characteristics of Kaifeng Pagoda, Architecture Science, **24**, (03), 2008, pp15–24. [In Chinese]
20. MILANI, G., LOURENCO, P. B., and TRALLI, A. Homogenised Limit Analysis of Masonry Walls, Part I: Failure Surfaces, Computers and Structures, **84**, (3-4), 2006, pp166–180.
21. RECCIA, E., CAZZANI, A., and CECCHI, A. FEM-DEM Modeling for Out-of-plane Loaded Masonry Panels: A Limit Analysis Approach, The Open Civil Engineering Journal, **6**, (1), 2012, pp.231–238.
22. PEPE, M., PINGARO, M., TROVALUSCI, P., RECCIA, E. and LEONETTI, L. "Micromodels for the In-plane Failure Analysis of Masonry Walls: Limit Analysis, FEM and FEM/DEM Approaches", Frattura ed Integrità Strutturale, **14**, (51), 2019, pp504–516.
23. MILANI, G., LOURENÇO, P., and TRALLI, A. 3D Homogenized Limit Analysis of Masonry Buildings under Horizontal Loads, Engineering Structures, **29**, (11), 2007, pp3134–3148.
24. Investigation Report on the Status Longhu Pagoda in Deyang, Sichuan Province, China, Chinese Cultural Heritage Research Institute, 2011. [In Chinese]
25. JC/T 796-1999: JC/T 796-1999 Method for Evaluating the Grade of Sintered Ordinary Brick by Rebound Tester, PRC, 1999. [In Chinese]
26. Research on the Determination of the Grade of Brick on the Wall by Rebound Method and the Evaluation of Brick Wall Masonry Quality by Ultrasonic, Shaanxi Provincial Architectural Research and Design Institute. [In Chinese]
27. JGJ 136-2001: JGJ 136-2001 Technical Regulations for Testing the Compressive Strength of Masonry Sand by Penetration Method, 2001. [In Chinese]
28. GB 5003-2001: GB 5003-2001 Code for Design of Masonry Structures, 2001. [In Chinese]
29. HABIEB, A. B., MILANI, G., TAVIO, T., and MILANI, F. Low Cost Frictional Seismic Base-Isolation of Residential New Masonry Buildings in Developing Countries: A Small Masonry House Case Study. The Open Civil Engineering Journal, **11**, (1), 2018, pp1026–1035.
30. WANG, P., SCACCO, J., MILANI, G., and LI, S. Seismic vulnerability evaluation of Longhu pagoda, sichuan, PRC. Proceedings of the International Conference on Structural Dynamic, EURODYN 2020, **2**, 2020, pp4226–4242.
31. DE IASIO, A., WANG, P., SCACCO, J., MILANI, G., and LI, S. Longhu pagoda: Advanced numerical investigations for assessing performance at failure under horizontal loads. Engineering Structures, **244**, (June), 2021, pp112715.
32. GB 50011: GB 50011 Code for Seismic Design of Buildings, PRC, 2016. [In Chinese]
33. SeismoArtif User Guide, © 2002-2020 Seismosoft Ltd.
34. SeismoSignal User Guide, © 2002-2020 Seismosoft Ltd.
35. WANG, P., and MILANI, G. Specialized 3D Distinct Element Limit Analysis approach for a fast seismic vulnerability evaluation of massive masonry structures: Application on traditional pagodas, Engineering Structures, In press, 2023.
36. MILANI, G., LI, S., and WANG, P. Fast seismic vulnerability evaluation of Wenfeng Pagoda in Yangzhou, PRC. AIP Conference Proceedings, 2293, 2020, pp5–9.
37. WANG, P., DE IASIO, A., SCACCO, J., MILANI, G., and Li, S. Full 3D CAD procedure for the limit analysis of longhu Pagoda in China. COMPDYN Proceedings, 2021, pp398–405.
38. WANG, P., SCACCO, J., MILANI, G., and LI, S. Seismic vulnerability evaluation of longhu pagoda, sichuan, prc. Proceedings of the International Conference on Structural Dynamic, EURODYN, **2**, 2020, pp4226–4242.
39. WANG, P., MILANI, G., SCURO, C., DEMARCO, F., OLIVITO, R. S., and LI, S. Simulation and Fast vulnerability analysis of a Chinese masonry pagoda. Journal of Physics: Conference Series, 2204(1), 2022.

On The Effective Stiffness of Slender Concrete Masonry Walls in the Canadian Masonry Standard

M. BOGOSLAVOV[(1)] and N.G.SHRIVE[(2)]
[(1)] *Department of Civil Engineering, University of Calgary, Calgary, Alberta, T2N 1N4, Canada*
mihailo.bogoslavo1@ucalgary.ca
[(2)] *Professor, Department of Civil Engineering, University of Calgary, Calgary, Alberta, T2N 1N4, Canada,*
ngshrive@ucalgary.ca

ABSTRACT
The Canadian masonry design standard (code of practice) can be particularly conservative when it comes to the design of walls deemed slender. One of the major contributors to the conservatism is the definition of the effective flexural stiffness of the wall. The effective stiffness is a term which can be used in linear analysis to determine the flexural displacement of a wall accounting for the fact that the wall may be cracked in the zone of high moment and thus the stiffness is actually non-uniform over its height – the effective stiffness essentially averages the actual stiffness over the height. An experimental test program performed in the mid-1970s at the University of Alberta, in which the lateral displacement profiles of the walls tested were recorded at increasing loads up to failure, was used to evaluate the current provisions of the standard and to develop a better equation to define the stiffness. The equation derived involves the eccentricity of the applied axial load as well as the slenderness of the wall. The approach to determining the equation is described together with reasons why some walls showed higher effective stiffnesses than that calculated for an uncracked section. The proposed equation is applicable to the data set analysed and further work needs to be done to determine if it has wider applicability.

KEYWORDS: concrete blockwork, walls, slenderness, effective stiffness.

1. INTRODUCTION

The design of slender masonry walls using the Canadian masonry design standard [1] (equivalent to a code of practice for the design of structural masonry in other countries) has been shown to be overly conservative [2,3]. Müller et al. [2] analyzed the results of nine test programs in which slender walls were loaded axially and at times laterally and tested to failure. Comparisons were made between the experimental failure loads of the walls to predicted failure loads as per the Canadian Standard [1]. The underestimation in design capacity in the slender wall design provisions in the Standard was demonstrated and the inaccuracy shown to be more significant for taller walls and lower axial load eccentricities. Isfeld et al. [3,4] extended the work and showed through modelling that many walls were failing with the mortar joints not displaying any flexural cracking (mortar and units remaining in full contact) (Table 1) – not as expected from a flexural or buckling mode of failure.

Slender walls are identified in the standard by their effective height to thickness ratio and are expected to be subject to significant secondary moments. Primary moments are applied at the ends of the wall (e.g. through eccentricity of axial load) whereas secondary moments develop through the height of the wall, being the axial load multiplied by the lateral displacement of the wall as it deforms horizontally. Thus, secondary moments amplify the effects of primary moments.

Walls for which slenderness effects are to be considered are expected to experience out-of-plane failure, in contrast to “short” walls which are expected to experience material failure. The Standard [1] requires slenderness effects to be considered when:

$$kh/t \geq (10 - 3.5(\frac{e_1}{e_2})) \quad (1)$$

where kh is the effective height of the wall which depends on the support conditions at the top and bottom; t is the wall thickness and e_1 and e_2 are the eccentricities of the axial load at the top and bottom of the wall respectively. So, for example, a wall with the required minimum eccentricity of axial load at the top and bottom of t/10 on the same side of the centre-line, is considered slender if the effective height to thickness ratio exceeds 6.5. Thus, a wall constructed of 200mm concrete block is considered slender once the height reaches 1.3m. That is, a seven course (1.4m) high wall 200mm wide is expected to undergo out-of-plane failure when loaded at an eccentricity of one-tenth of the thickness, top and bottom, whether hollow or fully grouted. A wall so loaded would be subject to compression across the whole section, so flexural failure would not occur, and the Euler buckling load is about twenty times greater than the load that would cause compressive failure in the outermost compressed fibre. The conservatism is evident. Further evidence of the inaccuracy of the standard in predicting slender wall behaviour is provided in the tests of Hatzinikolas et al. [5,6]. These authors tested walls that were all considered slender by the standard but show two types of failure – compression and flexure. Analysis of the reported displacements of the walls, presented in part here, confirms non-flexural failure in some cases, demonstrating further the need for the relevant clauses in the standard to be reconsidered.

The standard also specifies that a slender wall with kh/t less than 30 may carry 80% of the axial capacity of the wall, whereas if the slenderness is greater than 30, then only 10% of the axial capacity is permitted. This step change in permissible load is in stark contrast to the equivalent clauses in many other standards where the allowable axial load decreases as a continuous function of slenderness, as illustrated for TMS 402/602-22 [7] and EC6 [8] in Figure 1. The inconsistency needs to be addressed as walls with slenderness just under 30 might be at risk of failure while those with slenderness just over 30 are inefficient in their use of the material.

The use of wall thickness to define slenderness rather than radius of gyration is perhaps a consequence of rules developed for solid brickwork. In a solid section, the radius of gyration is √12 (3.46) times the thickness. Thus, the point of division of 30 in Figure 1 for the Canadian standard is the same as approximately 100 if radius of gyration were used.

Table 1
State of bed joints at masonry wall failure for pinned-pinned fully grouted concrete masonry walls subject to different load eccentricities, as per Isfeld et al. (2019): c = closed (no flexural cracking), p = partially open (flexural cracking partway across a joint), f = full opening (cracking right the way across a joint with point contact remaining)

Wall h/t	e/t = 0	e/t = 1/10	e/t = 1/6	e/t = 1/4	e/t = 1/3	e/t = 1/2.5	e/t = 1/2
5	c	c	c	c	p	f	f
10	c	c	c	c	p	f	f
20	c	c	c	p	p	f	f
30	c	c	c	p	f	f	f
40	c	c	c	p	f	f	f
60	c	f	f	f	f	f	f

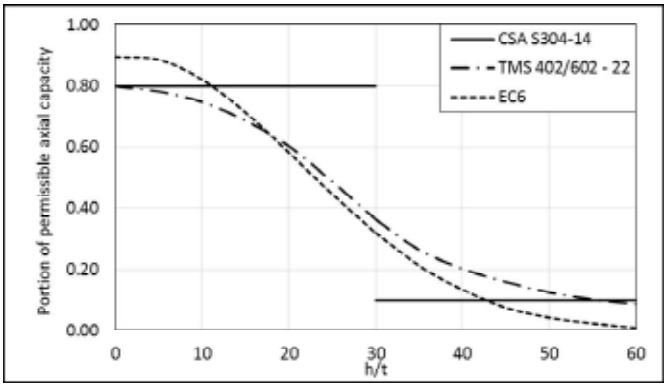

Figure 1 Permissible axial loads as a function of slenderness ratio (defined here as height to thickness) for three different international standards, CSA S304-14 [1], TMS402/602-22 [7] and EC6 [8]

Two methods are described in the standard [1] to account for the secondary moment, moment magnifier and Pδ. The moment magnifier is expressed as:

$$M_{ftot} = M_{fp}\frac{C_m}{1-\frac{P_f}{P_{cr}}} \geq M_{fp} \quad (2)$$

where M_{ftot} is the total moment (accounting for the secondary moment). M_{fp} is the primary moment calculated from the initial axial and lateral loads and P_f is the initial axial load. P_{cr} is the critical axial compressive load defined in the standard as:

$$P_{cr} = \pi^2\phi_{sr}(EI)_{eff}/[(1+0.5\beta_d)(kh)^2] \quad (3)$$

where EI_{eff} represents the effective flexural stiffness and serves to account for the loss of wall cross-section utilized in resisting bending as the wall cracks in the high moment area. Thus, EI_{eff} is an average stiffness over the height of the wall accounting for the fact that part of the wall has cracked. As such EI_{eff} provides the lateral displacement of the wall when used in standard linear elastic displacement calculations. β_d is the ratio of the total factored dead load moment to total factored moment and Φ_{sr} is the resistance factor for the member stiffness used in the determination of slenderness effects on the capacity of reinforced masonry (a different factor ϕ_g is used for plain masonry). C_m is the moment diagram (shape) factor defined in [1] as:

$$C_m = 0.6 + 0.4M_1/M_2 \geq 0.4 \quad (4)$$

where M_1 and M_2 are the moments at the top and bottom of the wall, not respectively, but with $M_2 > M_1$.

Similarly, in the Pδ method, the lateral displacement of the wall, δ, is determined through repetitive linear elastic analysis starting with the initial uncracked stiffness, EI_0 (I_0 is the second moment of area of the uncracked section), determining the lateral displacement, adjusting the moment to include the secondary moment, recalculating the displacement and iterating with EI_{eff} until the secondary moment and lateral displacement are stable.

Thus, the accuracy of both methods depends on the accuracy of the estimation of the effective stiffness of the wall. In the standard [1], the effective stiffness is defined as:

$$(EI)_{eff} = E_m[0.25I_g - (0.25I_g - I_{cr})(\frac{e-e_k}{2e_k})] \quad (5)$$

for reinforced walls, but with the condition that EI_{eff} is less than $0.25E_mI_0$ and greater than E_mI_{cr}. E_m is the modulus of elasticity of the masonry, I_{cr} is the second moment of area of the cracked section and e_k is the kern eccentricity. For plain walls EI_{eff} is simply $0.4E_mI_0$.

Thus, for a given wall, the flexural stiffness can be one of two values – uncracked or effective. That is, it does not matter what the extent of cracking is caused by the primary and secondary moments, the stiffness is fixed. It would make much more sense that the effective stiffness depended on the loads and eccentricity, because those factors affect the extent of cracking and therefore how much the stiffness of the wall has changed from the uncracked state. The objective of the work described here therefore, was to develop a way of determining the effective stiffness of a genuinely slender wall based on the axial load applied and its eccentricity.

Given the concerns outlined above, the masonry industry in Canada is seeking to improve the Canadian design standard in respect of the design of slender walls. To that end, the industry has supported experimental tests in four universities across the country and theoretical work has been pursued. That work has progressed with the objective of creating a logical design procedure which allows designers to determine if a wall will fail in compression, flexure of through buckling. As the Euler buckling load involves the flexural stiffness of a wall, it remains important to predict the effective stiffness accurately: the work presented here is one step toward that goal.

2. METHOD

Various experimental programs [5-6,9-12] on slender concrete masonry walls were studied to see which provided suitable data for an assessment of the effective stiffness. Of these, only the Hatzinikolas et al. reports [5,6] had sufficient information for the intended analysis. Walls with different combinations of grout and reinforcement were tested. Details of the walls and their construction are presented in [5] with lateral displacements up the height of each individual wall presented in [6]. The concrete blocks used (stretcher units, half blocks, end blocks) had strengths of about 17N/mm^2. The walls were constructed with Type S mortar (1:0.5:4.5, Portland Cement: Lime: Sand) and coarse grout. The 28-day strength of the mortar was 17.5N/mm^2 with a coefficient of variation of 8.3%, whereas the grout had a strength of 16.4N/mm^2 with a coefficient of variation of 10.6%. Masonry prisms and short walls failed at various strengths from 10.3 to 14.4N/mm^2 depending on the presence and type of joint reinforcement and whether the specimens were fully or just face-shell bedded. Plain walls in the group analysed here were reported to have a strength of 12.6N/mm^2. The walls were from 12 to 22 courses in height and a metre wide (an end block, a stretcher block and a half block in each course, constructed in running bond).

All the walls were tested under pinned-pinned end conditions with various levels of axial load eccentricity: the same load eccentricity was applied at the top and bottom of each wall as it was tested. All the walls were deemed slender according to Equation (1). Only those walls subject to single curvature were analysed in this study. Only one of each combination of wall type and eccentricity was tested. Thus, for example, group B consisted of five walls nominally the same (same grouted area, same vertical reinforcement): of these five walls, one was tested when axial load was applied at each of the eccentricities of zero, t/6, t/3, 2t/5 and t/2. The walls analysed are listed in Table 2. As may be seen in the table, use of the clauses in the Standard [1], including Equation (2), overestimate measured displacements by considerable amounts when axial load is applied at low eccentricity. The equations were more accurate with higher eccentricities.

Table 2
Hatzinikolas et al. [6] Recorded lateral deflection vs. calculated lateral deflection using CSA S304-14 [1]

Wall Name	Slenderness Ratio (m/m)	Vert. Reinf. (Imp.)#	Eccentricity (mm)	Failure Load (kN)	Recorded Test Deflection (mm)	Calculated Deflection (mm)	Calculated (CSA S304-14) to Test Deflection Ratio
A1	13.8	Plain	19.4*	1246	1.3	25.4	19.5
A2	13.8	Plain	32.3	708	7.0	16.5	2.4
A3	13.8	Plain	64.5	357	10.0	13.8	1.4
A4	13.8	Plain	19.4*	1068	1.0	18.9	18.9
A5	13.8	Plain	76.2	116	8.0	4.8	0.6
B1	13.8	3#9	19.4*	1868	4.0	655.7	163.9
B2	13.8	3#9	32.3	1423	10.2	110.5	10.9
B3	13.8	3#9	64.5	622	26.7	37.7	1.4
B4	13.8	3#9	76.2	689	26.7	52.0	2.0
B5	13.8	3#9	88.9	511	19.1	39.3	2.1
C1	15.9	3#9	19.4*	890	1.0	37.3	37.3
C2	15.9	3#9	19.4*	1601	1.0	26.2	26.2
C3	15.9	3#9	32.3	1110	16.5	127.1	7.7
C4	15.9	3#9	64.5	556	25.6	49.1	1.9
C5	15.9	3#9	76.2	545	42.0	56.1	1.3
C6	15.9	3#9	88.9	400	40.6	41.5	1.0
D1	18.0	3#9	19.4*	1068	2.5	364.7	145.9
D2	18.0	3#9	19.4*	1868	3.3	39.1	11.9
D3	18.0	3#9	32.3	890	24.0	143.0	6.0
D4	18.0	3#9	64.5	484	40.6	59.0	1.5
D5	18.0	3#9	76.2	420	48.3	55.1	1.1
D6	18.0	3#9	88.9	369	53.3	52.7	1.0
H1	18.0	3#6	19.4*	1868	0.1	54.7	1215.9
H2	18.0	3#6	32.3	1154	15.0	56.5	3.8
H3	18.0	3#6	64.5	384	34.3	157.5	4.6
H4	18.0	3#6	76.2	290	43.2	134.1	3.1
H5	18.0	3#6	88.9	249	57.0	181.2	3.2
I1	18.0	3#3	19.4*	1423	0.1	41.7	1042.2
I2	18.0	3#3	32.3	965	16.5	47.2	2.9
I3	18.0	3#3	64.5	240	3.0	82.2	27.4
I4	18.0	3#3	76.2	146	4.0	67.8	16.9
I5	18.0	3#3	88.9	108	9.0	110.7	12.3
L1	24.3	3#9	19.4*	1868	15.0	71.3	4.8
L2	24.3	3#9	32.3	667	18.0	42.6	2.4
L3	24.3	3#9	64.5	400	76.2	142.7	1.9
L4	24.3	3#9	76.2	356	79.0	124.9	1.6
L5	24.3	3#9	88.9	326	96.0	120.2	1.3
M1	24.3	Plain	19.4*	623	5.0	95.8	19.2
M2	24.3	Plain	32.3	534	25.0	87.1	3.5

#Imperial bar sizes convert to metric in a soft sense as: #3 being akin to a metric #10, a #6 to a metric #19 and a metric #9 to a #29.
*In this case axial load was applied concentrically, but as per CSA S304-14 [1] a minimum eccentricity of 19.4mm (0.1t) is assumed for the calculation. Hatzinikolas et al. [5,6] used blocks with a 194mm thickness (nominal 8 inch blocks with actual width 7⅝ inches): such blocks are not commonly used in Canada today

The uncracked flexural stiffness of each wall type was calculated from the wall geometry and the material properties presented in [5]. Then, given the lateral displacements provided, P_{cr} and the effective stiffness of the wall could be determined for each load step where the displacement profile was presented. Equations (3), (4) and (5) were used as appropriate with linear analysis for the displacement. Iteration is required for a solution, but the effective stiffness for that specimen subject to the specified load can be determined. Results like those shown in Figure 2 were obtained for all relevant sets of data. As in Figure 2 for the wall loaded at an eccentricity of t/6, some sets showed that for walls subject to loads at low axial eccentricity there was no change in the effective stiffness with increasing axial load. Indeed, occasionally, the initial effective stiffness was one of the lowest values! It was clear therefore, that for these specimens, there was not progressive cracking from flexure.

Indeed, Hatzinilolas et al. [5] note that the walls failed in one of two fashions and examination of pictures in their report confirm that one mode was flexural with the wall displacing laterally and joints opening on the tension side of the wall, while the other was compressive failure with multiple cracking parallel to the height of the wall. Walls like C3 (tested at an eccentricity of t/6) appeared to fail in compression with little lateral displacement, as may be seen in Figure 3. The walls loaded at t/6 had small lateral displacements, so the apparent flexural stiffness changes little with increasing load, even apparently doing the impossible and increasing as the load increased. Typically, the walls loaded at a low axial load eccentricity were deflecting less than is predicted in the deflection equation for a given load. This was because when the eccentricity fell within the kern, the load had to be a large proportion of the axial capacity before any cracking occurred and a secondary moment developed and at that point most of those walls experienced significant drops in their EI_{eff} values. When walls that clearly flexed were analysed, given the displacement profiles presented in [6], results shown in Figures 4 to 6 were obtained. Note that in some instances, increased flexural stiffness was determined for some of these walls at very low loads – possibly due to the accuracy of the instrumentation and the experimental arrangement. Figures 4 to 6 reveal the importance of eccentricity and the fact that the flexural stiffness declines as the load increases. That is, the stiffness decreases as the lateral displacement and the amount of cracking increase. In all cases the stiffness has fallen to about 40% of the uncracked stiffness as the load reaches about 40% of the critical load.

With the relevant data plotted in Figures 4 to 6, an iterative approach was employed to obtain an appropriate logarithmic function to describe the change in stiffness with load. The objective was to create an algorithm that slightly underestimated the effective stiffness for each load increment for a set of walls which had axial load applied at the same eccentricity but were of varying slenderness ratios. The approach was something between trial and error and a formal Newton-Raphson analysis. A more sophisticated curve fitting approach was not employed because the aim was not to create an equation to provide the best approximation of the values of the effective stiffness term, but rather to underestimate the stiffness at each load increment and thus provide a conservative estimate. Additionally, due to the sample size used for this analysis as well as the lack of variability in material and construction (as only walls used from the Hatzinikolas et al. [5] testing program were analyzed), it was deemed sufficient simply to iterate for the most appropriate equation. A logarithmic function most accurately followed the curve of the relationship between normalized axial load vs. normalized effective stiffness.

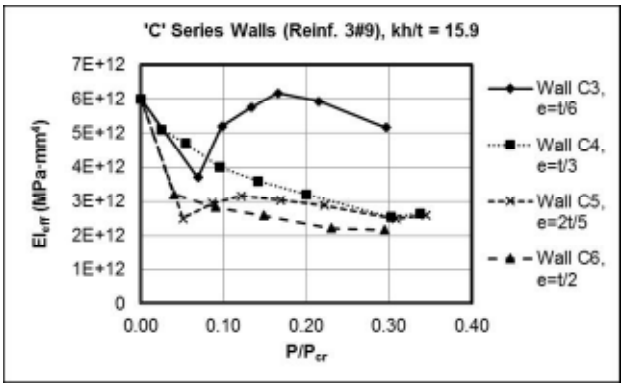

Figure 2 P/P_{cr} vs. EI_{eff} – Hatzinikolas et al. [5, 6] program wall series 'C'

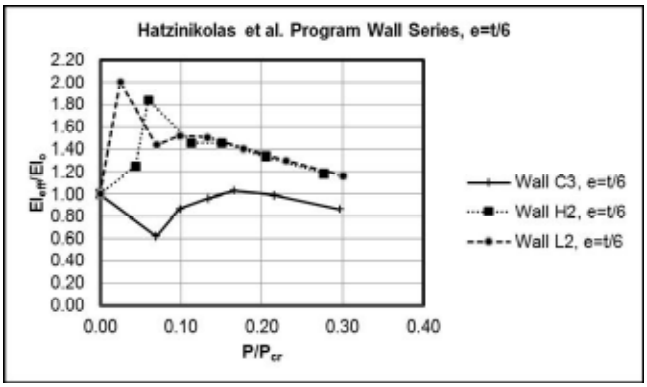

Figure 3 P/P_{cr} vs. EI_{eff}/EI_o plot for walls loaded at an axial load eccentricity of t/6

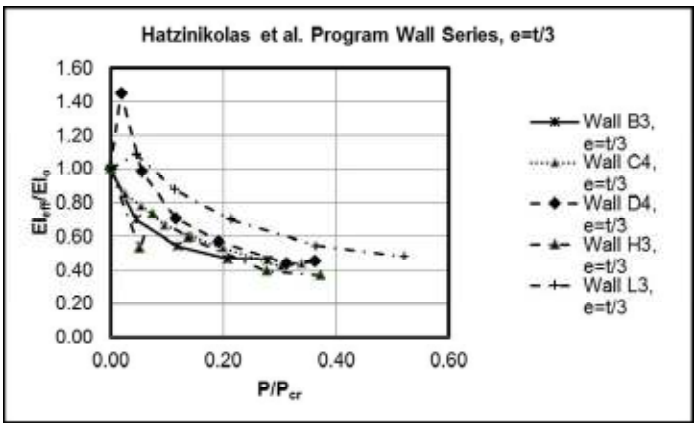

Figure 4 P/P_{cr} vs. EI_{eff}/EI_o plot for walls loaded at an axial load eccentricity of t/3

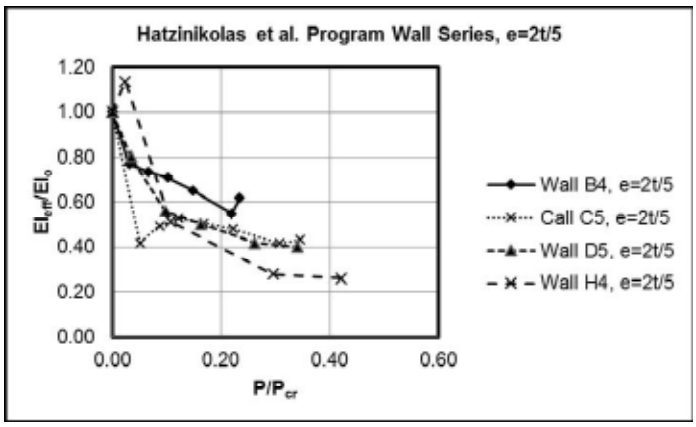

Figure 5 P/P_{cr} vs. EI_{eff}/EI_o plot for walls loaded at an axial load eccentricity of 2t/5

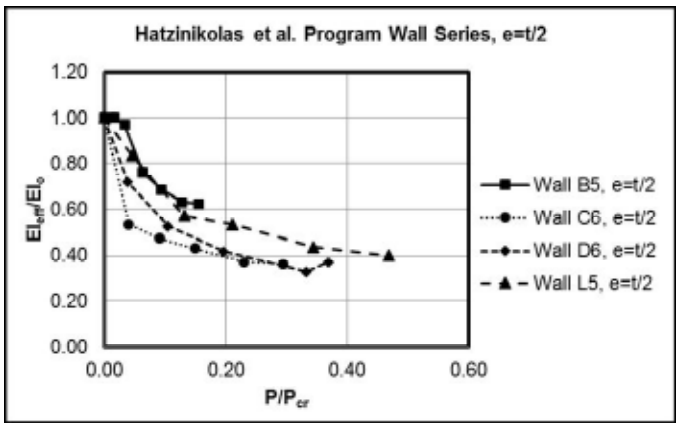

Figure 6 P/P_{cr} vs. EI_{eff}/EI_o plot for walls loaded at an axial load eccentricity of t/2

3. RESULT

The following equation was determined as being appropriate for the objective of the work:

$$\frac{EI_{eff}}{EI_o} = -\left(0.05 * \left(\frac{t}{e}\right)\right)\ln\left(\frac{P}{P_{cr}}\right) + 0.2, \quad EI_{eff} \leq EI_o \qquad (6)$$

Where EI_{eff} is the effective stiffness, EI_o is the original stiffness of the wall, t is the wall thickness, e is the axial load eccentricity, P is the applied axial load and P_{cr} is critical buckling load as determined with Equation (3).

The result of using this equation may be seen in Figures 7, 8 and 9. The value of 0.2 was added to the equation after being adjusted to ensure the selected equation just minimally underestimates the effective stiffnesses at the load points. To account for the shape of the function varying as the axial load eccentricity is changed, a shape factor was introduced to the equation in the form (0.05*t/e). The value of 0.05 was selected as providing the most appropriate shape of the equation relative to the available data points. The points below the function at low loads are not of concern as the data points at low loads were highly variable, on both the up and down sides of effective stiffness as mentioned before. Points for walls H3 and H4 in Figures 7 and 8 fall just below the proposed relationship and it is not evident from the reports [5,6] why the stiffness of these walls degraded slightly more than the stiffness of other walls. The majority of points are above the curves from the proposed equation and thus the equation is deemed to be satisfactory.

4. DISCUSSION

It is clear from the numerical results presented by Isfeld et al. [3] and the results of the Hatzinikolas et al. testing [5,6] that not all walls deemed slender by the Canadian masonry design standard [1] fail by flexure or buckling. The standard appears conservative in many instances and out of step with other standards in terms of its provisions. Hatzinikolas et al. [5] show that walls loaded axially at low eccentricities failed through material compressive failure while Isfeld et al. [3] predict similar behaviour with their modelling. Isfeld et al. also looked at fix-fix end boundary conditions which showed no joints being cracked at failure, up to slenderness of h/t = 60.

The standard therefore forces unnecessary over-design of many walls. A new approach should be considered in which the wall failure mode is considered in the first instance through examination of both the slenderness, preferably designated as the ratio of height to radius of gyration, axial load eccentricity and lateral load on the wall. In this context, the proposed equation could be used to determine a more accurate effective stiffness value for walls which are deemed to fail in flexure, rather than walls expected to experience material failure (based on their slenderness, axial load eccentricity and lateral loads).

Finite element models of walls with and without lateral loads were used to assess the degree to which the lateral loads affect the walls' failure mode and capacity [13]. The applied lateral loads represented average Canadian wind pressures as per the National Building Code of Canada [14]. Unreinforced and ungrouted concrete block walls with height to thickness ratios (h/t = 10, h/t = 20, h/t = 30 and h/t = 40) were modelled. In particular, the study focused on wall models which were loaded at low axial load eccentricities to determine whether these walls failed by material compressive failure even with the applied lateral load, as would have been expected after reviewing the results from Isfeld et al. [3] and Hatzinikolas et al. [5,6]. Wall models were loaded at axial loads eccentricities of 0, one tenth of the wall thickness and one sixth of the wall thickness. Most walls tested as part of the Hatzinikolas et al. testing program which were loaded at an axial load eccentricity of one sixth of the wall thickness did not experience a significant reduction in flexural stiffness and experienced a material compressive failure. This is consistent with the fact that for a solid wall, an eccentricity of one sixth of the wall thickness is the edge of the kern and axial load applied within this eccentricity should lead only to compressive stresses over the cross-section. In their modelling, Ahmed et al. [13] found that all joints were closed at failure except in the case of h/t being 40, with the axial load at e = t/6 and lateral wind load. In this latter case some joints were partially open (partially cracked) at ultimate load. Without the lateral load, all joints remained closed. Once the likely wall failure mode has been identified, the wall should be designed against the load that causes that failure, whether it be material compressive failure, flexure or buckling. Here, a flexural failure is one where the flexural tensile strength is exceeded on the outer tensile fibre leading to failure, whereas buckling implies instability leading to a large lateral displacement at constant load prior to failure.

5. LIMITATIONS

There are several limitations to this work. First and foremost is the lack of experimental data excepting the Hatzinikolas et al. work against which to judge the proposed equation. These authors only tested one of each type of specimen and loading. Further testing is therefore required in which the lateral displacement profile of the walls need to be recorded as a function of load. Such testing should include hollow concrete masonry walls as well as partially grouted walls. A shift in the Canadian standard to using radius of gyration rather than wall thickness, would remove the current penalty on these walls for having a larger radius of gyration than for a solid wall. Testing and/or modelling needs to be done with maximum wind loads rather than average so that clauses can be developed for the standard which are conservative. Further testing/modelling also needs to be completed with validated models to explore the effects of different strengths of masonry, the effects of different end eccentricities (the analysis for developing the proposed equation only considered walls subjected to the same end eccentricities) and the effects of double curvature. The literature needs to be examined to see whether the equation works with brickwork, and/or stonework, or whether separate equations are needed for these materials. In essence, the proposed equation is only applicable to the walls from which it was derived and further work is needed to show its applicability on a wider scale.

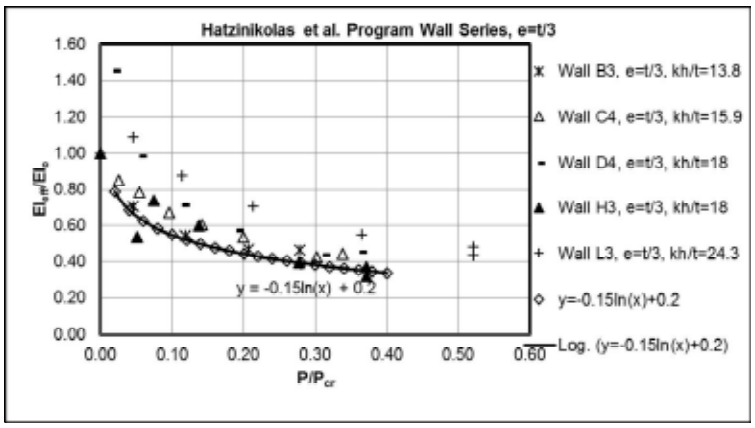

Figure 7 P/P_{cr} vs. EI_{eff}/EI_o plot for walls loaded at an axial load eccentricity of t/3

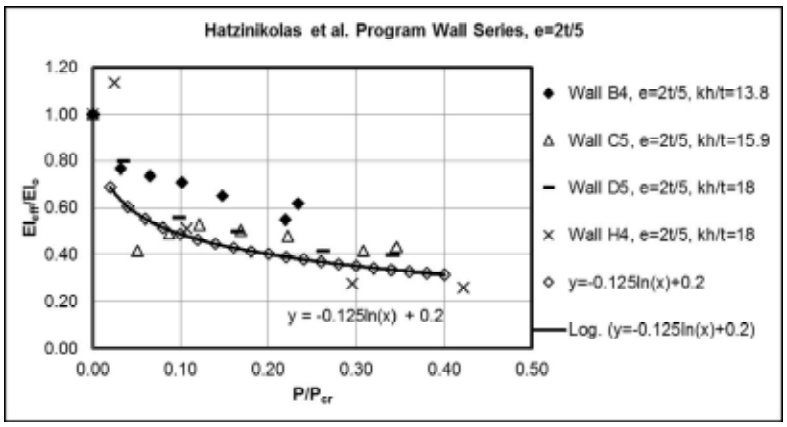

Figure 8 P/P_{cr} vs. EI_{eff}/EI_o plot for walls loaded at an axial load eccentricity of 2t/5

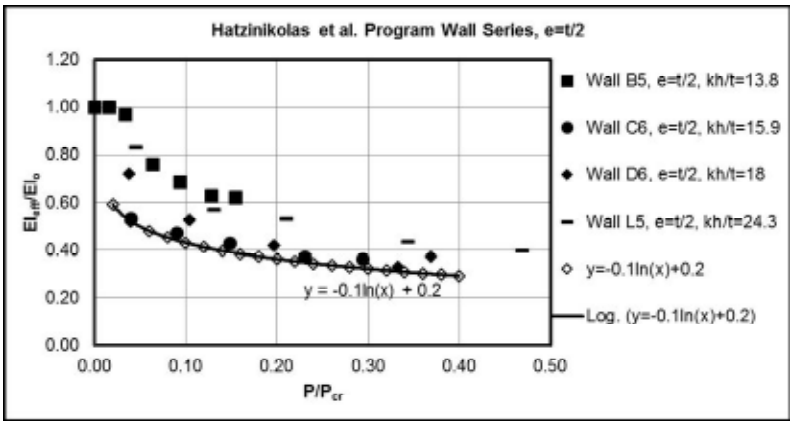

Figure 9 P/P_{cr} vs. EI_{eff}/EI_o plot for walls loaded at an axial load eccentricity of t/2

5. CONCLUSIONS

The Canadian masonry design standard is behind other standards in several respects when it comes to the design of slender walls. Improvement is required. One problem is the definition of the effective flexural stiffness which governs the estimated buckling load of a wall. Using the only set of comprehensive test data available, it has been possible to develop a conservative equation for that effective stiffness, which is a function of the applied load, and thus the extent of flexural cracking in a wall. Using this equation, both the buckling load and the lateral displacement of a wall can be estimated with greater accuracy than when using the current provisions in the standard.

ACKNOWLEDGEMENTS

The authors gratefully acknowledge the financial support of the Natural Sciences and Engineering Research Council of Canada and the University of Calgary.

REFERENCES

1. CANADIAN STANDARDS ASSOCIATION. Design of Masonry Structures, CSA S304.1-14, CSA Group, Mississauga, Ontario, Canada, 2014.
2. MÜLLER, A.L., ISFELD, A.C., HAGEL, M. and SHRIVE, N.G. Review and Analysis of Capacity of Slender Concrete Masonry Walls, Proceedings, 13th Canadian Masonry Symposium, Halifax, Paper 43, 2017 11pp.
3. ISFELD, A.C., HAGEL, M. and SHRIVE, N.G. Finite Element Analysis of Hollow Concrete Block Masonry Walls, Proceedings, 13th North American Masonry Conference, Salt Lake City, 2019 pp1110-1122.
4. ISFELD, A.C., MÜLLER, A.L., HAGEL, M. and SHRIVE, N.G. Analysis of Safety of Slender Concrete Masonry Walls in Relation to CSA S304-14, Canadian Journal of Civil Engineering, 46, (5), 424–438, 2018.
5. HATZINIKOLAS, M., LONGWORTH, J. and WARWARUK, J. Concrete Masonry Walls, Structural Engineering Report No. 70. University of Alberta, Edmonton, AB, Canada, 1978a.
6. HATZINIKOLAS, M., LONGWORTH, J. and WARWARUK, J. Experimental Data for Concrete Masonry Walls, Structural Engineering Report No.71, University of Alberta, Edmonton, AB, Canada, 1978b.
7. THE MASONRY SOCIETY. TMS402/602- Building code requirements and specifications for masonry structures, Boulder Colorado, USA, 2022.
8. EUROPEAN COMMITTEE FOR STANDARDIZATION, EN 1996-1-1. Eurocode 6. Design of Masonry Structures. Part 1-1: common rules for reinforced and unreinforced masonry structures, Brussels, Belgium, 2005.
9. YOKEL, F.Y., MATHEY, R.G. and DIKKERS, D.R. Compressive Strength of Slender Concrete Masonry Walls, National Bureau of Standards, USA, 1970.
10. YOKEL, F.Y., MATHEY, R.G. and DIKKERS, D.R. Strength of Masonry Walls Under Compressive and Transverse Loads, National Bureau of Standards, USA, 1971.
11. ACI-SEASC Task Committee on Slender Walls. Test Report on Slender Walls, ACI Southern California Chapter/Structural Engineers Association of Southern California, Los Angeles, California, 1982.
12. LIU, Y. and HU, K. Experimental Study of Reinforced Masonry Walls Subjected to Combined Axial and Out-of-Plane Bending, Canadian Journal of Civil Engineering 34, (11), 1486-1494, 2007.
13. AHMED, A., ISKANDER, G., BOGOSLAVOV, M., ISFELD, A. and SHRIVE, N.G. Examining the Mode of Failure of Slender Concrete Block Walls. Proc., 14th Canadian Masonry Symposium, Montreal, 2021 11pp.
14. NATIONAL RESEARCH COUNCIL OF CANADA. National Building Code of Canada. Canadian Commission on Building and Fire Codes, Ottawa, Ontario, Canada, 2015.

Characterizing Bidirectional Interaction in Unreinforced Masonry Buildings by Pseudo Dynamic Hybrid Simulation

KRISHNACHANDRAN S [(1)], XU HUANG [(2)], OH-SUNG KWON [(2)] and ARUN MENON [(3)]
[(1)] *Research Scholar, Department of Civil Engineering, IIT Madras, Chennai, India*
krishnchandran@gmail.com
[(2)] *Post Doctoral Fellow, Department of Civil and Mineral Engineering, University of Toronto, Canada*
xu.huang@mail.utoronto.ca
[(2)] *Professor, Department of Civil and Mineral Engineering, University of Toronto, Canada*
os.kwon@utoronto.ca
[(3)] *Professor, Department of Civil Engineering, IIT Madras, Chennai, India*
arunmenon@iitm.ac.in

ABSTRACT
Seismic analysis requires consideration of bidirectional loading components which have been shown to be more critical compared to unidirectional excitations. Bidirectional loading histories tend to reduce the actual capacity of structural members and accelerate their strength and stiffness degradation. With respect to unreinforced masonry (URM) buildings, bidirectional interaction has been an area in which limited experimental research has been carried out to date. In this regard, no quasi-static tests have been undertaken to study the effect of bidirectional interactions and therefore no loading protocol which represents the failure of URM buildings under bidirectional loading has been established. Hence, the existing numerical models have not been validated for their capacity to capture the interaction response of masonry piers. This study looks at employing the novel testing methodology of pseudo dynamic hybrid simulation to investigate the effect of bidirectional interaction on the response of unreinforced masonry piers. In this approach, the unreinforced masonry pier is modelled analytically in the host computer and experimentally tested simultaneously. The numerical model communicates with the experimental specimen to obtain the unknown response parameters which cannot be characterized by the numerical model independently. Accordingly, the combined numerical-experimental response provides the complete response of the structural member. Results suggest that there is considerable difference between the response of an unreinforced masonry pier under unidirectional and bidirectional loading in terms of strength capacity, stiffness degradation and hysteresis energy dissipation. Also, pseudo dynamic hybrid simulation provides valuable indicators regarding the future course of testing protocols for capturing bidirectional interaction in URM buildings.

KEYWORDS: Unreinforced masonry, Pseudo-dynamic testing, Hybrid simulation, Bidirectional interaction

NOTATIONS

x_d Displacement response of secondary system
$\ddot{x}_g$ Ground acceleration
x_w Displacement response of primary system
x_{ip} In-plane displacement
x_{oop} Out-of-plane displacement
k_{xd} In-plane Stiffness of secondary system along global x direction
k_{yd} In-plane Stiffness of secondary system along global y direction
k_{xw} In-plane Stiffness of primary system along global x direction
k_{yw} In-plane stiffness of primary system along global y direction
k_{oxw} Out-of-plane stiffness of out-of-plane walls along global x direction
k_{oyw} Out-of-plane stiffness of out-of-plane walls along global y direction
m_w Seismic mass of primary system
m_d Seismic mass of the secondary system
m_{oop} Out-of-plane wall mass
m Idealized seismic mass
c_{ip} Damping in the in-plane direction
c_{oop} Damping in the out-of-plane direction

1. BACKGROUND

The components of seismic load paths in an Unreinforced Masonry (URM) building are as shown in Figure 1. At any floor level, the seismic response of an URM building can be considered as a combination of the response of in-plane walls, which can be termed as the primary system; and the diaphragm and out-of-plane walls, termed the secondary system. For rigid floor diaphragms, the displacements and accelerations at each point in the diaphragm will be the same and equal to the response of the supporting in-plane walls, provided there is adequate connectivity between them. However, for flexible floor diaphragms, the response of the diaphragm will be different from that of the in-plane walls. Hence, a proper understanding of the interaction between components of the primary system and secondary system is essential for defining the overall seismic response of URM buildings. The primary system can be further discretized into vertical members called piers, horizontal members called spandrels and the connecting link between piers and spandrels idealized as rigid nodes as shown in Figure 1.

URM buildings with flexible diaphragms can be considered as rigid wall-flexible diaphragm buildings. In classical building response idealization, the entire building responds as one single unit whose response is governed by the primary lateral load resisting elements which also include the diaphragms. In rigid wall-flexible diaphragm buildings, the overall seismic response will be dominated by the deformation of the flexible diaphragm thereby resulting in typical local failure modes in the form of out-of-plane wall detachments. Hence, the diaphragm and out-of-plane walls need to be considered as a separate secondary system. The deformation demand at the top of out-of-plane walls will be equal to the deformation of the diaphragm since they act in a combined manner constituting the secondary system (Figure 2).

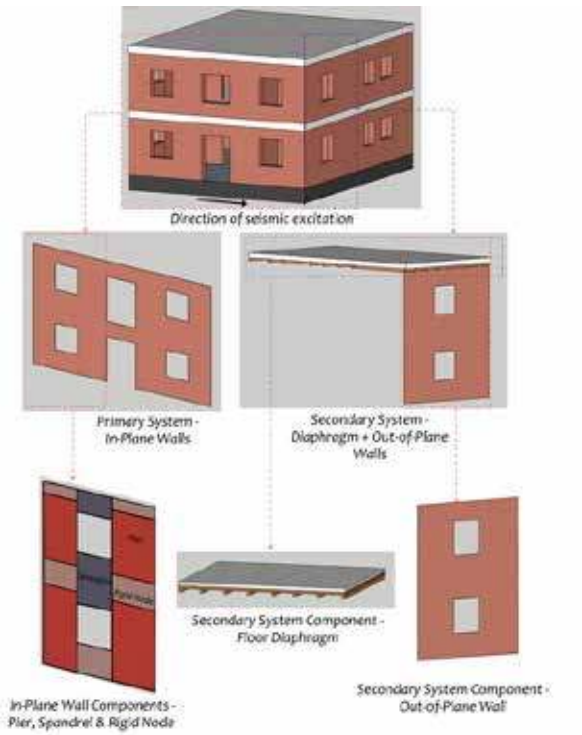

Figure 1 URM building - classification into primary system and secondary system

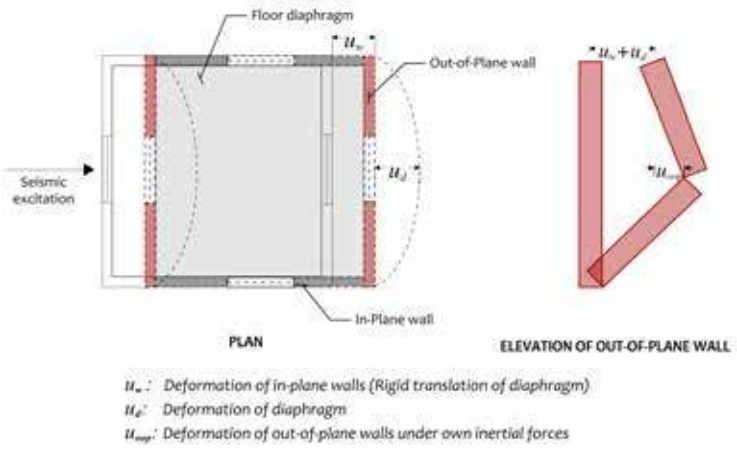

Figure 2 Deformation of floor diaphragms and out-of-plane walls

2. DYNAMIC RESPONSE OF URM BUILDINGS

The two-dimensional response (along the horizontal plane) of URM can be defined using 9 degrees of freedom as shown in Figure 3. This includes the displacement response of the primary system along the x and y directions (x_w and y_w) as the first two degrees of freedom (x_1 and y_1). Further, the displacement response of horizontal floor diaphragms along the x and y directions (x_d and y_d) are considered as the next two degrees of freedom (x_2 and y_2). The displacement response of out-of-plane walls along the x and y directions (x_{oop} and y_{oop}) are considered as the final translational degrees of freedom (x_3 and y_3). Further, there will be the rotation of the above three elements defined along the xy plane as the three rotational degrees of freedom (θ_1, θ_2, θ_3). The masses and stiffnesses corresponding to the above three elements (primary system/in-plane walls, diaphragms and out-of-plane walls) are denoted using m_w, m_d and m_{oop} and k_w, k_d and k_{oop} along both x and y directions.

Rotational degrees of freedom are not considered in this study, it is considered as a symmetric URM building which thereby reduces the 9 dof system to 6. This simplifies the analysis methodology to only addressing the problem of bidirectional interaction in URM buildings; the major aspect considered in this research. The x and y translational degrees of freedom of out-of-plane walls (corresponding to x_3 and y_3) are not considered as part of the global system. This is because the stability of out-of-plane walls can be considered independently in the assessment scheme using non-linear kinematic analysis or limit analysis methods as appropriate for the assessment of out-of-plane walls. However, in the presence of strong connections between the diaphragm and out-of-plane walls, there will be a critical contribution from out-of-plane walls as part of the secondary system in determining the deformation of the diaphragm (x_2 and y_2). This contribution from out-of-plane walls has been considered by including the mass and stiffness of the out-of-plane walls in the secondary system.

Figure 4 shows a URM building subjected to bidirectional seismic excitation. The displacement response at any floor level can be defined using the displacement at the top of in-plane walls (response of the primary system), denoted as x_w and the displacement of the floor diaphragm and out-of-plane walls (response of the secondary system), denoted as x_d. Accordingly, the equation of motion for the coupled response of the building at any floor level can be expressed as shown in Equation (1) [1]. The restoring force contribution from damping is not considered in these equations, owing to the simplification in representation. Accordingly, from Equation (1), the equation of motion for the response of the primary and secondary system can be defined using Equations (2) and (3) respectively:

$$\begin{bmatrix} m_{xw} & 0 \\ 0 & m_{xd} \end{bmatrix} \begin{Bmatrix} \ddot{x}_w \\ \ddot{x}_d \end{Bmatrix} + \begin{bmatrix} [k_{xw}] + [k_{xd} + k_{oyw}] & -[k_{xd} + k_{oyw}] \\ -[k_{xd} + k_{oyw}] & [k_{xd} + k_{oyw}] \end{bmatrix} \begin{Bmatrix} x_w \\ x_d \end{Bmatrix} = -\begin{bmatrix} m_{xw} & 0 \\ 0 & m_{xd} \end{bmatrix} \begin{Bmatrix} \ddot{x}_g \\ \ddot{x}_g \end{Bmatrix} \quad (1)$$

$$[m_{xw}]\{\ddot{x}_w\} + [k_{xw}]\{x_w\} + [k_{xw} + k_{oyw}](\{x_w\} - \{x_d\}) = -[m_{xw}]\{\ddot{x}_g\} \quad (2)$$

$$[m_{xd}]\{\ddot{x}_d\} + [k_{xd} + k_{oyw}](\{x_d\} - \{x_w\}) = -[m_{xw}]\{\ddot{x}_g\} \quad (3)$$

Traditionally, the seismic assessment of URM buildings has assumed rigid diaphragm constraints. When the diaphragm is rigid, the rigid wall-flexible diaphragm building idealization cannot be used and the entire building responds as one single system, classical box-action. Hence, the displacement response of the building will be defined only in terms of the response of the in-plane walls as shown in Equation (4), where 'm' represents the total seismic mass of the system. Thereby, the displacement response of the building will be defined only in terms of the response of the in-plane walls as:

$$[m]\{\ddot{x}_w\} + [k_{xw}]\{x_w\} = -[m]\{\ddot{x}_g\} \quad (4)$$

However, recent research has shown that for URM buildings with flexible/semi-rigid diaphragms, the response of the secondary system is equally important in the overall response of the structure, especially under bidirectional loading.

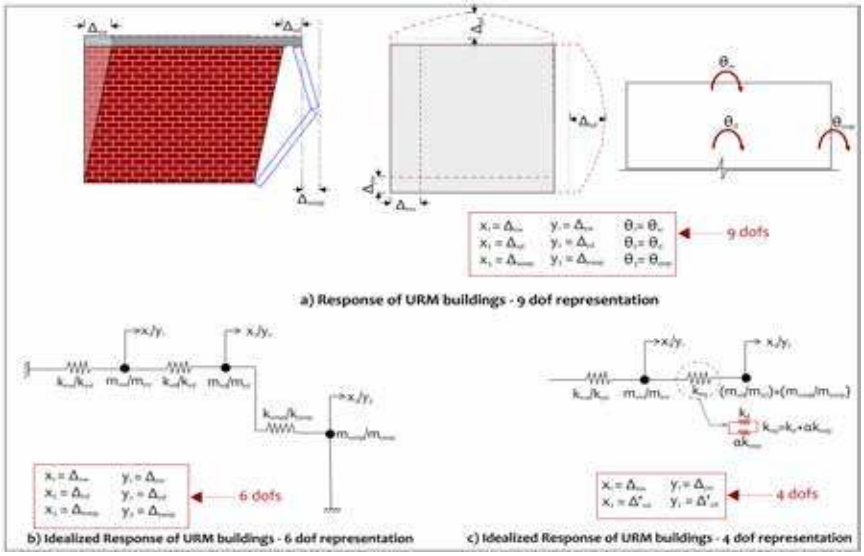

Figure 3 Analytical background for the primary-secondary system representation of URM buildings

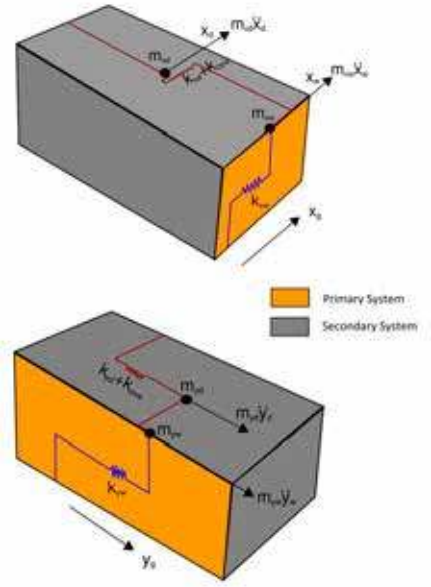

Figure 4 Idealization of URM building under bidirectional seismic excitation

3. BIDIRECTIONAL INTERACTION IN URM BUILDINGS

A critical aspect that has been neglected so far and which should be considered in the assessment of URM buildings is the effect of bidirectional loading. This effect has not been explicitly addressed due to the absence of well-defined failure mechanisms for URM buildings under bidirectional loading and also due to the simplification in performing the analysis. With respect to URM buildings, the seismic resistance is assumed to be derived only from the in-plane strength capacity of the walls. Out-of-plane strength capacity is not considered to be contributing to the seismic resistance of the structure. This is true under unidirectional loading, where each masonry wall will be part of either the primary system (as an in-plane wall) or the secondary system (as an out-of-plane wall) only. However, under bidirectional loading, the same wall will be a part of the primary system in one direction and the secondary system in the other, at the same time. The equations of motion along each direction of motion respectively can be defined as shown in (5) and (6):

$$\begin{bmatrix} m_{xw} & 0 \\ 0 & m_{xd} \end{bmatrix} \begin{Bmatrix} \ddot{x}_w \\ \ddot{x}_d \end{Bmatrix} + \begin{bmatrix} [k_{xw}] + [k_{xd} + k_{oyw}] & -[k_{xd} + k_{oyw}] \\ -[k_{xd} + k_{oyw}] & [k_{xd} + k_{oyw}] \end{bmatrix} \begin{Bmatrix} x_w \\ x_d \end{Bmatrix} = -\begin{bmatrix} m_{xw} & 0 \\ 0 & m_{xd} \end{bmatrix} \begin{Bmatrix} \ddot{x}_g \\ \ddot{x}_g \end{Bmatrix} \quad (5)$$

$$\begin{bmatrix} m_{yw} & 0 \\ 0 & m_{yd} \end{bmatrix} \begin{Bmatrix} \ddot{y}_w \\ \ddot{y}_d \end{Bmatrix} + \begin{bmatrix} [k_{yw}] + [k_{yd} + k_{oxw}] & -[k_{yd} + k_{oxw}] \\ -[k_{yd} + k_{oxw}] & [k_{yd} + k_{oxw}] \end{bmatrix} \begin{Bmatrix} y_w \\ y_d \end{Bmatrix} = -\begin{bmatrix} m_{yw} & 0 \\ 0 & m_{yd} \end{bmatrix} \begin{Bmatrix} \ddot{y}_g \\ \ddot{y}_g \end{Bmatrix} \quad (6)$$

It is important to note that k_{xw} and k_{oxw} are stiffnesses of the same wall along in-plane and out-of-plane directions respectively and stiffness degradation along one direction can impact the response in the other direction. Hence, it is important to view the wall as an element undergoing bidirectional response and investigate the effect of the out-of-plane response to the in-plane response of the wall and vice versa. To isolate bidirectional response of the primary system from that of the secondary system and to avoid the effect of coupling between the two, the responses of the primary system and secondary system were considered as statically uncoupled in this study. This results in the off-diagonal terms of Equations (5) and (6) becoming zero and getting reduced to Equations (7) and (8) respectively.

$$\begin{bmatrix} m_{xw} & 0 \\ 0 & m_{xd} \end{bmatrix} \begin{Bmatrix} \ddot{x}_w \\ \ddot{x}_d \end{Bmatrix} + \begin{bmatrix} [k'_{xw}] & 0 \\ 0 & [k_{xd} + k'_{oyw}] \end{bmatrix} \begin{Bmatrix} x_w \\ x_d \end{Bmatrix} = -\begin{bmatrix} m_{xw} & 0 \\ 0 & m_{xd} \end{bmatrix} \begin{Bmatrix} \ddot{x}_g \\ \ddot{x}_g \end{Bmatrix} \quad (7)$$

$$\begin{bmatrix} m_{yw} & 0 \\ 0 & m_{yd} \end{bmatrix} \begin{Bmatrix} \ddot{y}_w \\ \ddot{y}_d \end{Bmatrix} + \begin{bmatrix} [k'_{yw}] & 0 \\ 0 & [k_{yd} + k'_{oxw}] \end{bmatrix} \begin{Bmatrix} y_w \\ y_d \end{Bmatrix} = -\begin{bmatrix} m_{yw} & 0 \\ 0 & m_{yd} \end{bmatrix} \begin{Bmatrix} \ddot{y}_g \\ \ddot{y}_g \end{Bmatrix} \quad (8)$$

From (7) and (8), the bidirectional response of the walls oriented along the x direction can be shown as:

$$[m_{xw}]\{\ddot{x}_w\} + [k'_{xw}]\{x_w\} = -[m_{xw}]\{\ddot{x}_g\} \quad (9)$$

$$[m_{yd}]\{\ddot{y}_d\} + [k_{yd} + k'_{oxw}]\{y_d\} = -[m_{yd}]\{\ddot{y}_g\} \quad (10)$$

Hence, the response of a URM wall under bidirectional loading can be defined using Equations (9) and (10), where k'_{xw} and k'_{oxw} represent the updated in-plane and out-of-plane stiffness of the wall considering the effect of each on the other, termed “bidirectional interaction” in this research.

Bidirectional interaction in URM structures is a topic into which a very limited number of research investigations ([2-8]) have been undertaken. Among these, only a few studies have examined the effect of out-of-plane actions on in-plane capacity through experimental investigations ([2-3],[8]). However, all these tests were static monotonic in nature. Nevertheless, the results of these studies have shown that the attainment of in-plane strength capacity is limited by the presence of out-of-plane actions. Hence, ignoring the same could result in non-conservative capacity estimates for the structure.

Bidirectional loading tests on structural members show that the response is highly dependent on the loading pattern [9]. Any bidirectional loading history tends to reduce the actual capacity of a structural member and accelerate its strength and stiffness degradation. The response and failure modes of the structural elements are also path dependent in the case of bidirectional loading. Similar tests with different loading paths results in different damage progression [9]. Hence, the failure mode needs to be always correlated with the load path. Therefore, for capturing the effects of bidirectional loading, the choice of a realistic bidirectional loading protocol is of prime importance due to the response dependency of structural members on the imposed loading path. Researchers have employed a number of bidirectional loading paths for quasi-static tests, viz: diagonal, square, circular, ellipse etc. for studying bidirectional interaction problems. However, there is very little guidance available on which protocol is representative of the actual response during an earthquake due to the randomness in ground motion and variability in member response. URM piers have completely different responses and modes of failure along orthogonal directions. So far, a cyclic loading history which is representative of the damage evolution and the actual displacement path followed by URM buildings during seismic actions has not been established. Shake- table testing can simulate the seismic loads on the structure accurately by considering the inertial effects. However, to develop a loading history consistent with damage evolution and establish analytical relationships between the different parameters involved, will require the testing of many more specimens. To abrogate the need for numerous expensive laboratory tests, more sophisticated techniques need to be employed able to trace the real behaviour of URM buildings under bidirectional loading. Therefore, pseudo-dynamic testing is being resorted to which incorporates the advantages of shake table testing into quasi-static testing by implicitly accounting for the effect of dynamic loading.

4. PSEUDO DYNAMIC HYBRID SIMULATION

The Pseudo-Dynamic (PSD) test method is a computer-controlled testing technique that enables dynamic testing of structures in the non-linear range while using the same loading equipment that is used for quasi-static testing [10]. Using this method of hybrid simulation, the entire structure can be experimentally tested and modelled analytically on the host computer. The numerical simulation of the structure under dynamic loading is carried out based on the information measured directly from the experimental sub-structure as the experiment progresses. It also allows for more sophisticated tests where a portion of the structure is experimentally tested (sub-structuring) while the rest of the structure is analytically modelled which enables significant simplification for MDOF systems.

Although PSD tests have been adopted in tackling a variety of problems ([10-14]), the novelty of using these for bidirectional interaction studies is well accepted. The primary motivation for employing PSD tests to study bidirectional interaction effects is the dependence of damage evolution on the bidirectional loading protocol in quasi-static tests. One of the first pseudo-dynamic tests implemented in Japan [15] was to address the effect of bidirectional interaction in reinforced concrete moment resisting frames. It was understood that the coupling effects of orthogonal ground motion amplifies the response and realistic behaviour cannot be obtained from static tests alone. In addition, the validity of the numerical models to account for bidirectional interaction effects necessitated the use of pseudo-dynamic tests to study the effects of the bidirectional response in different structural systems. These included the study of elastomeric bearings subjected to coupled bidirectional response effects ([16-17]), bidirectional response of multi-storied reinforced concrete buildings ([18]), strength and stiffness degradation of RC bridge piers under bidirectional loading ([19-20]), Buckling Restrained Brace Frames ([21-23]), post-tensioned column with energy dissipators ([24]) etc.

With respect to URM buildings, PSD tests have been carried out for different objectives. Pacquette and Bruneau [25] employed PSD tests to study the interaction between a flexible floor and rigid wall in URM buildings. Anthoine and Molina [26] carried out PSD tests to assess the earthquake resistance of modern masonry constructions in central/northern Europe. Wenfeng et al. [27] used PSD tests for investigating the efficacy of retrofitting masonry residential buildings with precast steel reinforced concrete walls.

Hybrid simulation refers to the process of integrating substructure responses, captured on different platforms (experimental or numerical) so as to obtain a combined system response. It is resorted to, particularly in cases where:

a) The full scale experimental setup to capture an entire system's response is cumbersome and hence the system is sub structured into multiple components and their individual responses are integrated together. The entire process of conducting experimental tests for capturing unknown component behavior and incorporating the experimentally obtained response in a numerical model is achieved through a single hybrid simulation.
b) A numerical model for representing a component response is unavailable and how the component interacts with the global system needs to be captured.

The main components for executing hybrid simulations are:

4.1 Integration Module (IM): These are the main software modules in which the majority of the structural system are modelled. These communicate with the substructure module using a communication link established between them.

4.2 Sub-structure Module (SM): The sub-structure module is the module which is extracted out of the structural system for communicating with the integration module. For numerical hybrid simulation, this element is modelled in detail in the same/separate software platform. For experimental hybrid simulation, the specimen is experimentally tested with commands coming from the integration module and responses sent back to the same. This consists of the Interface Programme, Data Acquisition System, Actuator Controller and the actuator (Figure 5). The interface program, called the Network Interface for Controllers (NICON) [28] receives commands from the network based on a standardized data exchange format (UTNP), converts the received digital displacement command from IM to analog voltage signals and sends it to the actuator controller through a NI Data Acquisition Device (NIDAQ) which can generate analog input/output signals. The analog signal is then sent to the actuator and applied on to the specimen as actuator stroke displacements.

4.3 Communication: This consists of the communication protocol (rule by which the Integration Module communicates with the Substructure Module) and the data exchange format. The data exchange library compiled in any of the languages to facilitate communication between IM and SM.

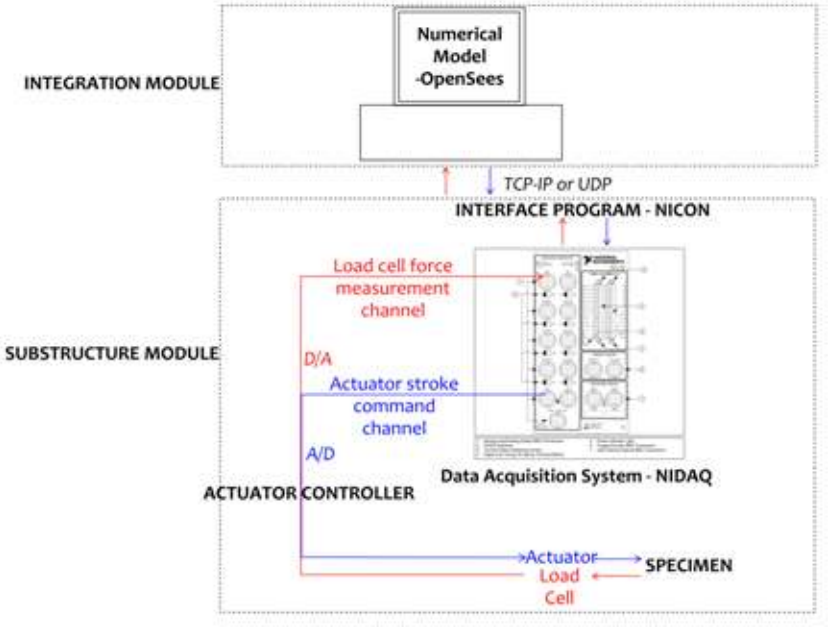

Figure 5 Hybrid simulation - architecture

5. METHODOLOGY

To study bidirectional interaction response in URM buildings using PSD testing, the geometry of the experimental specimen was fixed based on a typical URM wall with opening as shown in Figure 6. The thickness of pier was chosen as 230mm (representing the standard thickness of a one brick thick wall in a single story URM building). The pier geometry was configured based on Figure 6 which illustrates the pier spandrel idealization typically adopted in URM buildings.

There are infinite possible displacement paths for a URM pier to undergo when subject to bidirectional displacement cycles. Among them, the three direct paths are:

1. In-plane displacement followed by out-of-plane displacement
2. Out-of-plane displacement followed by in-plane displacement
3. Simultaneous in-plane and out-of-plane displacements

The problem addressed in this research work when an URM is under bidirectional interactions is the effect of out-of-plane displacements on the in-plane capacity since the lateral resistance for URM walls is derived from the in-plane direction. For these reasons, load path 2 would not be applicable to the current research and the choice would be between load path 1 and load path 3. Under bidirectional ground motion, the system is more likely to choose load path 3, over load path 1, because it is associated with the least energy for moving to the displaced configuration.

The URM pier which is a part of both the primary and secondary system is defined by Equation (9) along the in-plane direction and Equation (10) along the out-of-plane direction. Accordingly the integration module and substructure module for PSD testing is defined as shown in Figure 7. The integration module consists of the numerical model as a mass-spring-dashpot system along both in-plane direction and out-of-plane direction.

Two PSD tests were carried out using the substructure module corresponding to a URM pier governed by a flexural rocking mechanism. The first one (Unidirectional PSD test) corresponds to a unidirectional hybrid simulation where the secondary system is ignored and only the primary system is modelled and analysed in the IM. Hence, for the first PSD test, the mass-spring-dashpot system in Figure 7 is modelled only in the in-plane direction and the substructure element is subjected to in-plane displacements only. For the second PSD test (bidirectional PSD test), both the primary system and secondary system were modelled and the substructure element is subjected to both in-plane and out-of-plane displacements. The results of unidirectional PSD tests and bidirectional PSD tests could be used for comparing the responses of the pier under unidirectional and bidirectional loading respectively.

The governing equations of motion are Equation (10) in the in-plane direction and Equation (11) in the out-of-plane direction in the PSD test, with damping forces also considered in the equation of motion (c_{ip} and c_{oop} respectively as shown in Figure 7.

$$[m_{xw}]\{\ddot{x}_w\} + [c_{ip}]\{\dot{x}_w\} + [k'_{xw}]\{x_w\} = -[m_{xw}]\{\ddot{x}_g\} \quad (11)$$

$$[m_{yd}]\{\ddot{y}_d\} + [c_{oop}]\{\dot{y}_d\} + [k_{yd} + k'_{oxw}]\{y_d\} = -[m_{yd}]\{\ddot{y}_g\} \quad (12)$$

Further, the experimental module (sub-structure module) consists of the physical specimen. For the first time-step, in the integration module, Equations (11) and (12) are solved using a predefined in-plane and out-of-plane initial stiffness which is close to the corresponding stiffness of the pier. Accordingly, the displacements corresponding to the primary system response and secondary system response are obtained. These displacements are applied on the pier in the in-plane and out-of-plane direction respectively. Load cells will be connected to both the in-plane and out-of-plane actuators for measuring the restoring forces at the end of Step 1. The restoring forces will be measured in both directions during the application of these displacements.

For the second time-step, for both the primary system response and secondary system response, Equations (11) and (12) are solved with restoring forces obtained in Step 1 from the load cells in the experimental sub-structure. Following this, the displacements obtained by solving Equations (11) and (12) are applied on the sub-structure module. At the end of Step 2, the restoring force is measured from the load cell and fed back to the numerical model to be incorporated in the equations for Step 3. Thus, for each time-step, the restoring forces in both the in-plane and out-of-plane directions are measured and the equations of motions are updated with these restoring forces. Hence, the updated stiffness in both the in-plane and out-of-plane directions is represented in the respective equations of motion thereby representing the actual response of the pier during bidirectional excitation.

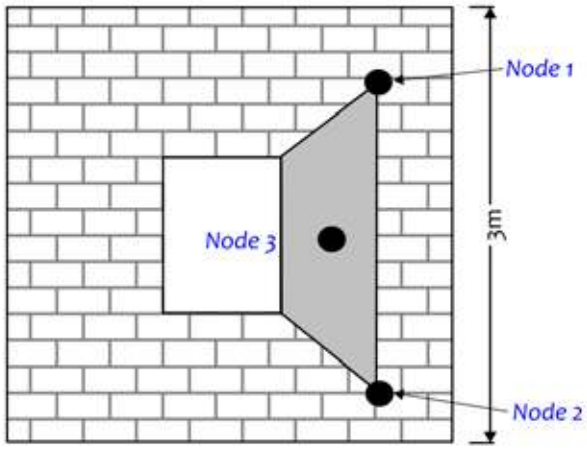

Figure 6 URM wall - macroelement definition

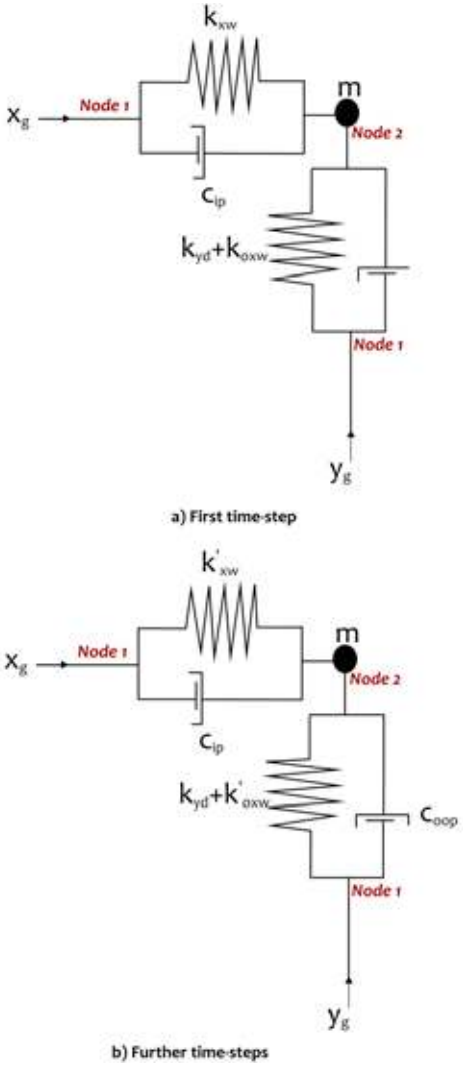

Figure 7 Integration module – OpenSees

Table 1
Mechanical properties (Sub-structure module)

Material Properties	Values
Young's Modulus (MPa)	2100
Poisson's Ratio	0.25
Mass Density (kN/m^3)	19
Tensile Strength (MPa)	0.15
Tensile Fracture Energy (N/m)	7
Compressive strength (MPa)	4.75
Compressive Fracture Energy (N/m)	15180

6. NUMERICAL HYBRID SIMULATION

Initially, numerical hybrid simulation was carried out to simulate the experimental PSD tests numerically. This was to set the modelling parameters for the integration module and ensure that the communication loop between the integration module and sub-structure module is functioning properly.

6.1 Integration module

The integration was modelled in OpenSees as it is and the sub-structure module was simulated using a numerical model in OpenSees. The spring element representing the pier was modelled in OpenSees as an elastic spring with a stiffness corresponding to the cracked stiffness (50% of the stiffness) of the pier. The tributary mass on the pier for the primary system corresponds to 5.3 tonnes and for the secondary system, the mass corresponds to 4.7 tonnes, calculated from a typical URM model building. The numerical model for diaphragms (represented by k_{yd}) is explained elsewhere [29].

6.2 Sub-structure module

The sub-structure element was modelled in OpenSees using the 3 noded macroelement by Vanin et al. [30]. The material properties adopted are summarized in Table 1.

Non-linear pushover analysis of the pier was carried out in OpenSees to obtain the capacity curves for the substructure element in both the in-plane and out-of-plane directions. The capacity curve of the pier obtained is shown in Figure 8. Results show that the failure mechanisms (rocking in the out-of-plane direction and flexural toe compression in the in-plane direction) were adequately captured by the macro model. Small differences (in the range of 25-30%) in the capacity estimates are expected for macro element-based models compared to the experimental specimens. This is mainly due to the simplified macro modelling approach where homogenization of material properties is adopted for modelling a non-homogeneous material like masonry.

6.3 Communication and feedback loop

Ground motion records corresponding to the Montenegro seismic event at the station Veliki Ston-F-Ka Soli (Record sequence number: 4459) was adopted for the PSD tests. The Montenegro earthquake event of 1979 is considered as relevant in the study of URM structures and for the development of assessment protocols for the same. In addition, the frequency content of the ground motion matches with the time period of unreinforced masonry buildings. Therefore, a significant number of the shake-table tests carried out in the study of unreinforced masonry buildings have adopted the Montenegro record as the input ground motion ([31-33]). The principal frequency contents (2-10Hz) of the Montenegro ground motion (PGA = 0.22g) matches with the typical period of URM buildings and allows a reliable comparison of results. Even though this is not a dynamic test and hence, frequency content of the ground motion does not affect the experimental substructure, it is important to make sure that the ground motion adopted for this study causes damage to short period rigid buildings like URM buildings. Therefore, the response spectrum of the ground motion was plotted and it is observed that the dominant frequency of the ground motion lies between 2Hz to 10Hz. The time period of the model building falls within this range and hence this choice is validated. The peak amplitudes of the ground motion resulting in inelasticity in the structure are covered within the first 5 seconds which makes it ideal for carrying out pseudo-dynamic testing considering the timescale to be adopted for the test.

Accordingly, the integration module was subjected to the ground motion and network communication was established with the substructure module for restoring force feedback. A Newton Raphson algorithm with an Alpha OS integrator was used in the analysis with an α value of 0.9. Rayleigh damping was considered in the model with stiffness proportional damping with the damping ratio considered as 2% for unreinforced masonry structures. Results of the analysis are detailed below.

7. EXPERIMENTAL HYBRID SIMULATION –TEST SETUP

7.1 Integration module

The integration module for experimental hybrid simulation was as explained in sections 5 and 6.

7.2 Substructure module

The test setup for the PSD tests consisted of the substructure element anchored to the test floor with no vertical pre compression applied on the test specimen. This was to simulate the case of lightly loaded piers typical of the top story of a URM building. Hydraulic actuators of 500kN capacity were used for applying the displacements obtained from the IM in both the in-plane and out-of-plane directions (Figure 9).

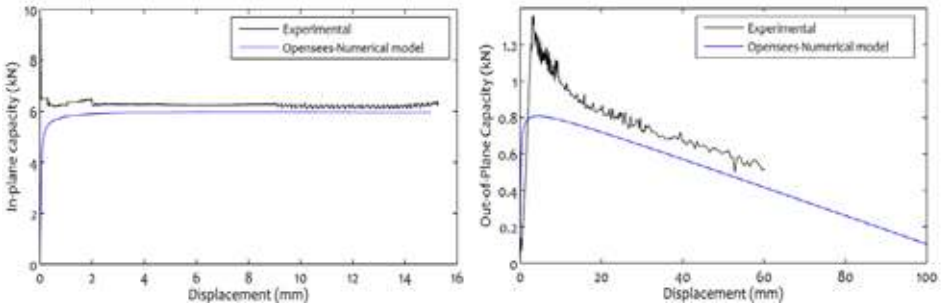

Figure 8 Numerical model calibration – capacity curves- in-plane (left), out-of-plane (right)

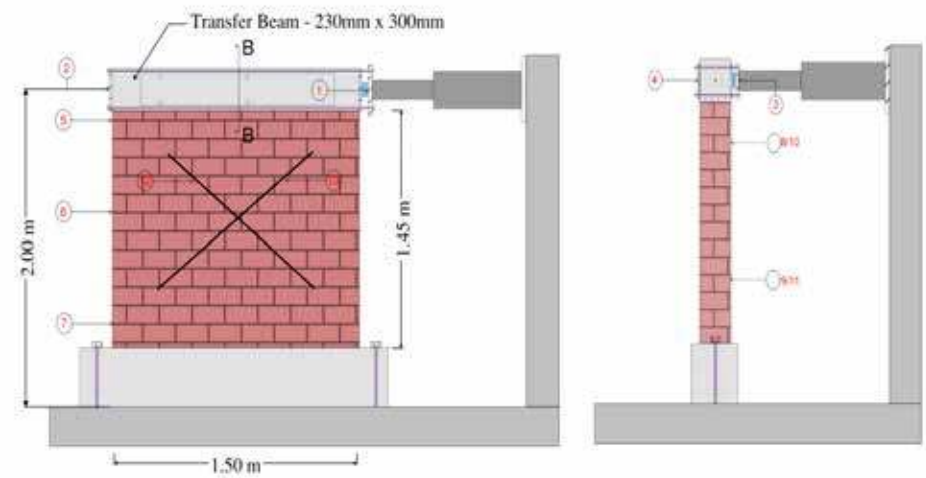

Figure 9 Experimental sub-structure – primary system (left), secondary system (right)

The details of the test setup are shown in Figure 9. Linear Variable Displacement Transducers (LVDTs) 1, 2, 5, 6 and 7 were used for the measurement of IP displacements. Among them LVDT 1 was used to measure the stroke displacement, i.e. displacement of the actuator and LVDT 2 was used to measure the specimen displacement corresponding to the actuator stroke. LVDTs 5, 6 and 7 measured the displacement at the top, mid-height and bottom of the specimen respectively. Similarly, LVDTs 3, 4, 8, 9, 10 and 11 were used for measuring the OOP displacements. LVDT 3 was used to measure the actuator stroke in the out-of-plane direction and 4 was used for measuring the corresponding specimen displacement. LVDTs 8, 9, 10 and 11 were placed symmetrically with respect to the centreline of the specimen at the top and bottom of the pier respectively. This was to check the possibility of torsional deformations in the out-of-plane direction. LVDTS 12 and 13 measured the shear deformation. The LVDTs had sensitivity for measuring up to 10-6mm.

7.3 Communication and feedback loop

The communication and feedback loop adopted in the test is detailed in Figure 5. However, the specimen deformation will not be the same as that of the applied stroke displacements due to the flexibility of the reaction system and connecting plates in the test setup. To account for these losses, an error compensation scheme is employed in NICON to ensure that the stroke displacement is modified so as to match the command displacement and specimen displacement. Accordingly, LVDTs 1 and 3 (in the in-plane direction and out-of-plane direction respectively) measure the actuator stroke displacement. The load cell measures the restoring force from the specimen and this is sent back to NIDAQ as analog voltage signals. These analog voltage signals are converted to digital by NICON, thereby estimating the restoring force in each cycle. Further, NICON sends the restoring force back to the integration module in OpenSees [34]. Thus one cycle is completed and this restoring force is adopted in the equation of motion for calculating the displacements in the IM in the next cycle.

8. RESULTS

The in-plane displacement histories of the pier in the unidirectional and bidirectional PSD tests are shown in Figure 10. The in-plane force-deformation hysteresis of the pier is shown in Figure 11. The experimental PSD test was carried out for the first 400 time steps for unidirectional loading and 200 time steps for bidirectional loading. This corresponds to 6 full cycles under unidirectional loading and 3 full cycles under bidirectional loading. The results of further time steps were not available due to various challenges with the actuator controller.

Results show that there is an appreciable effect of bidirectional loading on the response of the URM pier. It is already established from monotonic tests that there is a stiffness degradation and reduction in the toe crushing capacity of the pier due to bidirectional loading [8]. However, the bidirectional PSD tests show that not only the ultimate capacity, but also the rocking resistance is being reduced in each cycle due to the effect of bidirectional loading. Although the global failure mechanism in terms of flexural rocking was observed to be unchanged between unidirectional and bidirectional PSD tests, the method of resistance derived from the mechanism across the failure domain was observed to be altered. There is higher pinching effect and stiffness degradation even at low drift levels of 0.3%. This indicates that the hysteresis rule will invariably get altered under the effects of bidirectional loading. Under unidirectional loading, flexural rocking as a mechanism is associated with low levels of energy dissipation. However, this is not the case with the same mechanism under bidirectional loading.

A comparison of in-plane displacement histories under unidirectional and bidirectional loading (Figure 10) shows that the displacement response is amplified under bidirectional loading. A maximum in-plane displacement amplification corresponding to 30% was observed under bidirectional loading compared to the unidirectional loading scenario. This is mainly due to the reduced in-plane stiffness under bidirectional loading, further confirmed by Figure 11 which indicates that both unidirectional and bidirectional hysteresis loops were characterized by strength and stiffness degradation. In addition, softening of the hysteresis loop was observed for both cases. However, hysteresis pinching and increased energy dissipation during the cycles were observed for the bidirectional loading case. Pinching of hysteresis was due to the relative displacement of the masonry block along the failure plane. Unlike unidirectional loading where rocking and associated crack opening and closing are the only sources of energy dissipation, in bidirectional loading, the panel undergoes deformation in both in-plane and out-of-plane directions resulting in sliding of the macro block at the joint. For the in-plane response, the displacement in each cycle under the bidirectional PSD test was observed to be higher than the corresponding unidirectional test. This is due to the reduced stiffness and restoring force in each cycle during the bidirectional PSD test.

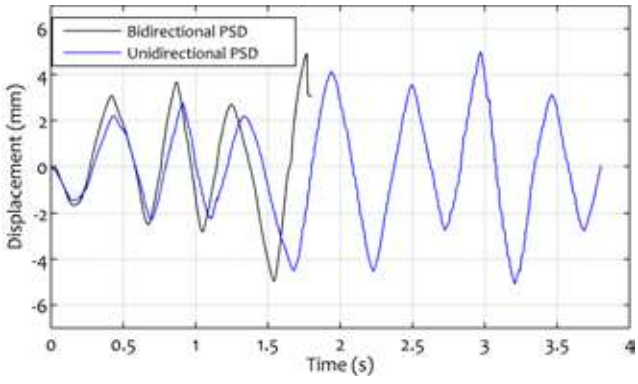

Figure 10 Displacement history - unidirectional vs bidirectional

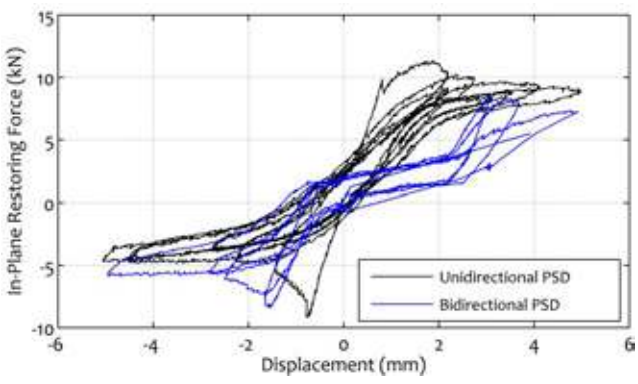

Figure 11 Force-displacement hysteresis - unidirectional vs bidirectional

Further, results from the numerical hybrid simulation for the bidirectional PSD test were compared with the experimental test results. The in-plane displacement history and out-of-plane displacement history from bidirectional PSD compared with the numerical hybrid test is shown in Figure 12(a) and 12(b) respectively. The results for the in-plane direction indicate that the displacement on the wall has been amplified in the experimental results compared to the numerical results. The maximum amplification was observed to be 105%. Since the existing numerical models do not account for the stiffness reduction in the in-plane direction due to out of plane displacements and vice versa, the predicted displacements from numerical PSD test are expected to be lower than the experimental PSD test. However, the effect was seen to be not as pronounced as observed for the displacement history in the out-of-plane direction (Figure 12(b)). For the out-of-plane direction, the displacement history was observed to be affected in terms of not only the peak amplitudes, but also the frequency content of the response. The out-of-plane response represents the response of the secondary system including the diaphragm and the out-of-plane response of the pier. Accordingly, drift orbit for bidirectional response was generated for both the experimental and numerical PSD test as shown in Figure 13. It shows that there is an amplification of the drift orbit due to the effect of bidirectional response, indicating that there is a reduction in in-plane stiffness due to out-of-plane displacements and also out-of-plane stiffness due to in-plane displacements.

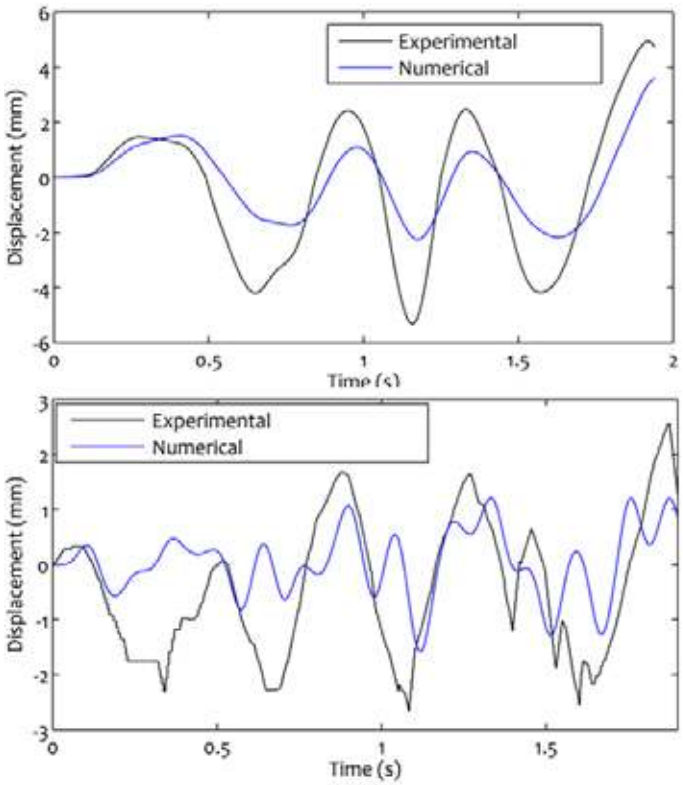

Figure 12 Displacement history - experimental vs numerical (a) in plane (top) b) out-of-plane (bottom)

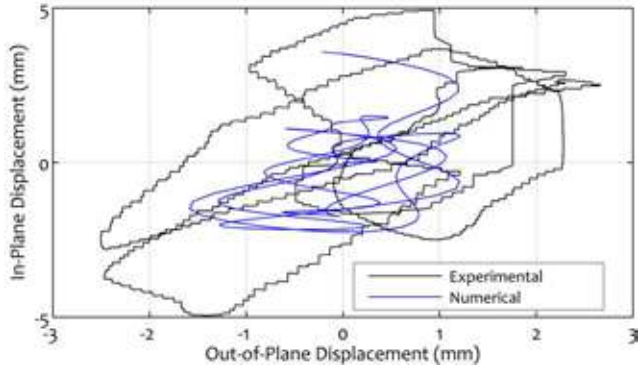

Figure 13 Drift orbit – experimental and numerical

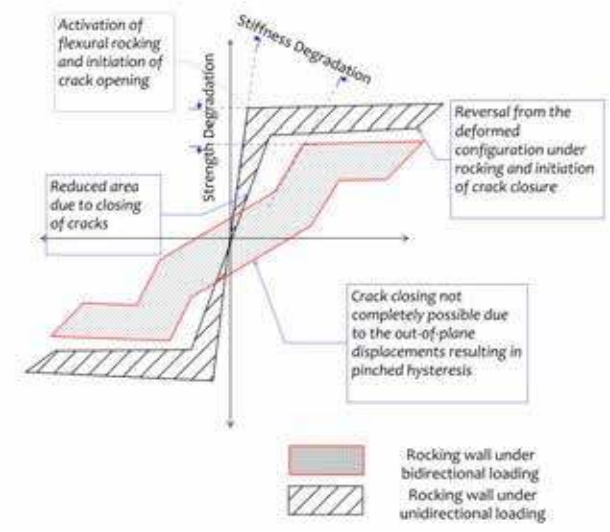

Figure 14 Idealized hysteretic response of rocking urm wall under bidirectional loading

9. DISCUSSION

Based on the results from the PSD tests, the rocking behaviour of URM walls under unidirectional and bidirectional loading is idealized as shown in Figure 14. In general, a rocking URM wall is characterized by a flag shaped hysteresis. The salient points of the curve are detailed in Figure 14. Once the wall undergoes cracking, rocking is initiated about the crack location followed by the opening of the crack with increased displacements. During load reversals, the closure of the crack initiates with reversal from the deformed configuration under rocking. Since the majority of the crack is closed during load reversal, the rocking mechanism is characterized by less hysteretic energy dissipation when the applied displacements are reduced. However, this may not be the case with bidirectional loading as shown in Figure 14. Since the wall is under out-of-plane cyclic displacements along with the in-plane cyclic displacements, a complete crack closure is not feasible under bidirectional loading. This results in a pinching of the hysteresis loop and increased hysteretic energy dissipation even when the in-plane displacements are a minimum. This could result in an accelerated strength deterioration at the cracked joint due to the combined loading effects, resulting in a net reduction in the effective area available for compression at the cracked joint. This further leads to a reduction in the restoring shear during the rocking mechanism thereby causing a decrease in the flexural capacity of the wall, as observed from the test results.

10. CONCLUSIONS

Bidirectional interaction in URM structures is a topic which has not been comprehensively addressed so far by existing research. For URM buildings, the most challenging aspect in a bidirectional loading scenario is the significant difference in the resisting mechanisms in the in-plane and out-of-plane directions which makes the choice of loading protocol critical. Hence, as a primary step, the evolution of failure domains in URM walls under bidirectional loading needs to be established. Pseudo dynamic testing has been a successful approach for capturing the interaction response in various structural members and the current set of studies signifies the same for URM walls as well. The results obtained provide valuable insights into the behaviour of piers under bidirectional loading. Degradation in strength capacity as well as stiffness was observed for URM piers under bidirectional loading. This is well represented by the bidirectional drift orbit which indicates an enlarged drift orbit under bidirectional loading. In addition, the hysteresis loop was also observed to be affected in terms of pinching of the loop resulting from the crack opening due to the combined effects of in-plane and out-of-plane loading.

11. LIMITATIONS

The scope of the current tests is limited by the number of time-steps and load cycles executed by the test specimen. A greater number of time-steps and load cycles up to the failure of the specimen would be required to trace the response of the element until failure. Hence, the current results should be considered only as an indicator for the response and evolution of the failure domain under bidirectional loading for rocking masonry piers. To quantify these in terms of a simplified analytical model, many more experimental tests and further detailed investigations need to be carried out.

REFERENCES

1. DERAKHSHAN, H., NAKAMURA, Y., GRIFFITH, M.C. et al. (2020). Simplified calculation of roof accelerations in existing low-rise symmetric unreinforced masonry buildings with flexible diaphragms. Bull Earthquake Eng **18**, pp 3383–3400. https://doi.org/10.1007/s10518-020-00823-1.
2. NAJAFGHOLIPOUR, M., MAHERI, M.R., LOURENCO, P. Definition of interaction curves for the in-plane and out-of-plane capacity in brick masonry walls,Construction and Building Materials **55**, 2014 pp 168–18.
3. DOLATSHAHI, K.M, AREF, A.J., WHITTAKER, A.S. Interaction curves for in-plane and out-of-plane behaviors of unreinforced masonry walls. Journal of Earthquake Engineering,**19(1)**, 2015. pp 60-84.
4. DOLATSHAHI, K.M., YEKRANGNIA, M., MAHDIZADEH, A. On the influence of in-plane damages on the out-of-plane behavior of unreinforced masonry structures. NCEE 2014 - 10th U.S. Natl. Conf. Earthq. Eng. Front. Earthq. Eng., 2014.
5. KOLLERATHU, J.A., MENON, A. Interaction of in-plane and out-of-plane responses in unreinforced masonry walls under seismic loads. Journal of Structural Engineering. **44**, 2017, pp 422–441.
6. NOOR-E-KHUDA, S., DHANASEKAR, M. Masonry Walls under Combined In-Plane and Out-of-Plane Loadings, Journal of Structural Engineering (United States*),* **144**, 2018, pp 1–10.
7. AGNIHOTRI, P, SINGHA,V, RAI D.C. Effect of in-plane damage on out-of-plane strength of unreinforced masonry walls. Engineering Structures; **57:1**, 2013, 10.1016/j.engstruct.2013.09.004.
8. KRISHNACHANDRAN, S, MENON, A. Effect of out-of-plane displacements on the in-plane capacity of lightly precompressed rocking unreinforced masonry piers. Engineering Structures, **281(1)**, 2023, 115756, https://doi.org/10.1016/j.engstruct.2023.115756.
9. RODRIGUES, H., VARUM, H., AREDE, A. et al. Behaviour of reinforced concrete column under biaxial cyclic loading—state of the art. International Journal for Advanced Structural Engineering **5(4),** 2013). https://doi.org/10.1186/2008-6695-5-4.
10. MOJIRI, S, KWON, O, CHRISTOPOULOS, C. Development of a ten-element hybrid simulation platform and an adjustable yielding brace for performance evaluation of multi-story braced frames subjected to earthquakes, Earthquake Engineering and Structural Dynamics; **48**, 2019, pp 749–771, https://doi.org/10.1002/eqe.3155.
11. WANG, X., KIM, R.E., KWON, O., YEO, I., and AHN, J. Continuous real-time hybrid simulation method for structures subject to Fire, Journal of Structural Engineering. **145**, 2019,. doi: 10.1061/(ASCE)ST.1943-541X.0002436.
12. KWON, O.S., KIM, H.-K., JEONG, U.Y et al. Design of Experimental Apparatus for Real-Time Wind-Tunnel Hybrid Simulation of Bridge Decks and Buildings, Structures Congress 2019, pp 235-245, 10.1061/9780784482247.022.
13. KAMMULA, V., EROCHKO, J., KWON, O.-S. and CHRISTOPOULOS, C. Application of hybrid-simulation to fragility assessment of the telescoping self-centering energy dissipative bracing system. Earthquake Engineering and Structural Dynamics. **43**, 2014, pp 811-830. https://doi.org/10.1002/eqe.2374.

14. HUANG, XU, BRODSKY, A. Multi-platform simulation of infilled shear-critical reinforced concrete frames subjected to earthquake excitations. Bulletin of Earthquake Engineering **20**, 2022, pp: 5323-5348.
15. SEKI, M, TESHIGAWARA, M., OKADA, T. Simulation of Earthquake Response of Reinforced Concrete Building Frame by Computer-Actuator On-Line System, Computational Methods and Experimental Measurements, 1982, pp 317-328, Springer Berlin H 5.
16. IWATA, S., IEMURA, H., AOKI, T., SUGIYAMA, K., UNO, Y. Hybrid earthquake loading test (pseudo-dynamic test) of bi-directional base isolation bearing for a large pedestrian bridge. Proceedings of the 10th Earthquake Engineering Symposium.**10-1**, 1998, pp: 207-212, 10.1007/978-3-662-11353-0_26.
17. MURAKOSHI, Y., IGARASHI, A., DANG, J, ITO, T. Bi-directional experimental hybrid simulations of elastomeric isolation bearings for validation of hysteretic modelling, 15th World Conference in Earthquake Engineering, Lisboa, 2012.
18. MOLINA, F.J., VERZELETTI, G., MAGONETTE, G., BUCHET, P., GERADIN, M. Bi-directional pseudo-dynamic test of a full-size three-storey building. Earthquake Engineering and Structural Dynamics, **28(12)**, 1999, pp 1541-1566.
19. HAYAKAWA, R., KAWASHIMA, K., WATANABE, G. Effect of bilateral loadings on the flexural strength and ductility of reinforced concrete bridge piers. JSCE Journal of Earthquake Engineering **27**, 2003, pp 1-4.
20. DHAKAL, R, MANDER, J.B, MASHIKO, N. Bidirectional Pseudo Dynamic Tests of Bridge Piers Designed to Different Standards. **12**, 2007, 10.1061/(ASCE)1084-0702(2007)12:3(284).
21. KHOO, H.-H., TSAI, K.-C., TSAI, C.-Y., WANG, K.-J. Bidirectional substructure pseudo-dynamic tests and analysis of a full-scale two-story buckling-restrained braced frame. Earthquake Engineering & Structural Dynamics 45(7), 2016, pp 1085–107.
22. QIYANG, T., BIN, W., PENGFEI, S., XU, G. et al. Experimental Performance of a Full-Scale Spatial RC Frame with Buckling-Restrained Braces Subjected to Bidirectional Loading, Journal of Structural Engineering, American Society of Civil Engineers, **147(3)**, 2021, doi.org/10.1061/(ASCE)ST.1943-541X.0002928.
23. VAZQUEZ-COLUNGA, S.Y., LEE, C.L, MACRAE, G.A. Bidirectional loading performance of gusset plates in buckling restrained braced frames, Engineering Structures **242**, 2021, doi.org/10.1016/j.engstruct.2021.112521.
24. GULTOM, R., MA, Q,T. Biaxial pseudo-dynamic tests of a post-tensioned rocking column with externally mounted energy dissipators. Proceedings of the 2015 NZSEE Annual Conference, 2015.
25. PAQUETTE, J., BRUNEAU, M. Pseudo-dynamic testing of unreinforced masonry building with flexible diaphragm and comparison with existing procedures,Construction and Building Materials **20(4)**, 2006, pp 220-228.
26. ANTHOINE, A., MOLINA, F.J. Pseudo-dynamic testing of full-scale masonry structures – Preparatory work, 14th International Brick and Block Masonry Conference, Sydney, 2008.
27. LI, WENFENG, WANG, TAO, CHEN, XI, ZHONG, XIANG, PAN, PENG. Pseudo-dynamic tests on masonry residential buildings seismically retrofitted by precast steel reinforced concrete walls. Earthquake Engineering and Engineering Vibration. **16**, 2017, pp 587-597. 10.1007/s11803-017-0397-6.
28. HUANG, XU, KWON, OH-SUNG. A Generalized Numerical/Experimental Distributed Simulation Framework, Journal of Earthquake Engineering, 24:4, 2020, pp 682-703, DOI:10.1080/13632469.2018.1423585.
29. VANIN, F., PENNA, A., BEYER, K. A three-dimensional macro-element for modelling the in-plane and out-of-plane response of masonry walls. Earthquake Engineering and Structural Dynamics **49**, 2020, pp 1365– 1387.
30. KRISHNACHANDRAN, S., MENON, A. Secondary system response in masonry buildings: Effect of integral wall-diaphragm response, Masonry International, International Masonry Society, UK, **35(1),** 2023, pp 12-19.
31. GUERRINI, G., SENALDI, I., GRAZIOTTI, F., MAGENES, G., BEYER, K., PENNA., A. Shake-Table Test of a Strengthened Stone Masonry Building Aggregate with Flexible Diaphragms, International Journal of Architectural Heritage, **13:7**, 2019, pp 1078-1097, DOI: 10.1080/15583058.2019.1635661.
32. SENALDI, I.E., GUERRINI, G., COMINI, P. et al. Experimental seismic performance of a half-scale stone masonry building aggregate. Bulletin of Earthquake Engineering **18**, 2020, pp 609–643.
33. GIARETTON, M., VALLUZZI, M.R., MAZZON, N. et al. Out-of-plane shake-table tests of strengthened multi-leaf stone masonry walls. Bulletin of Earthquake Engineering **15**, 2017, pp 4299–4317. https://doi.org/10.1007/s10518-017-0125-7.
34. MCKENNA, F. OpenSees: A Framework for Earthquake Engineering Simulation. Computing in Science and Engineering. **13**, 2011, pp 58–66.

Design & Print by: **Sherwin Rivers Ltd**, The Remer Printing Works, Waterloo Road, Stoke-on-Trent, ST6 3HR
Tel: 01782 212024 / Web: www.sherwin-rivers.co.uk / Email: sales@sherwin-rivers.co.uk

SUPPORTING THE CONSTRUCTION INDUSTRY

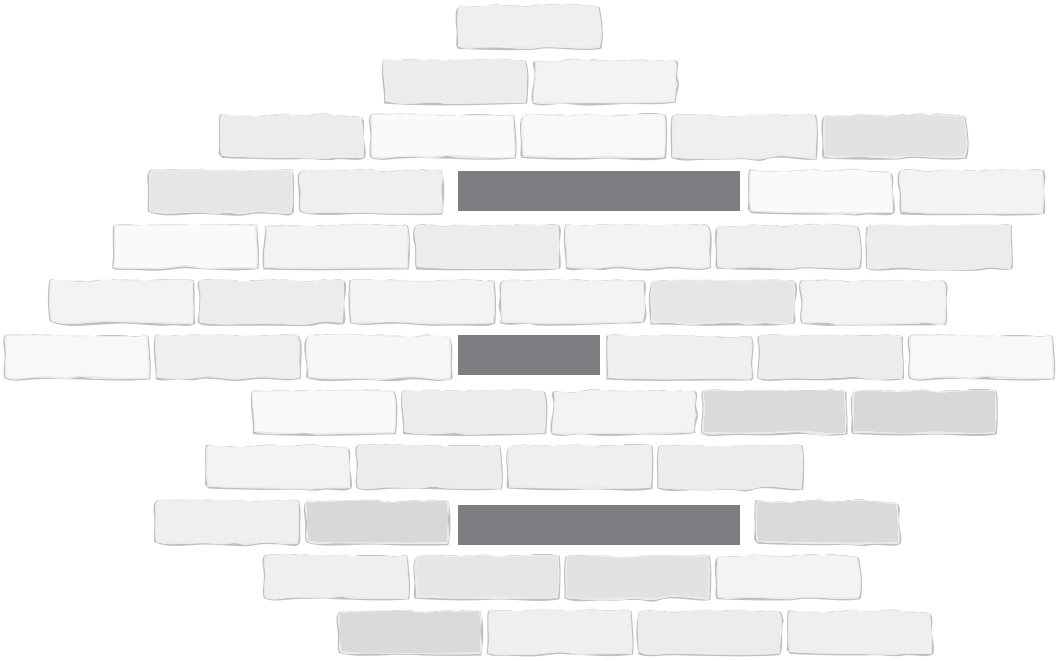

Materials • Products • Systems • Structures

We are experts in all things construction thanks to our extensive testing facilities, knowledge of current regulations and industry experience.

Our services include: materials classification, testing to international standards, product development, resource efficiency, structural and environmental testing and failure analysis. And this year we have added dynamic wind load testing.

Lucideon - helping clients to improve performance, solve problems, comply with regulations, meet specifications, realise projects, develop novel products/processes, and improve existing ones.

LUCIDEON

Materials Development • Testing • Assurance

Find out more at www.lucideon.com/mi

LUCIDEON - the new name for Ceram